THESIS

THE MANUFACTURING AND SOFT ROBOTIC APPLICATIONS OF FREE STROKE TWISTED AND COILED ACTUATORS

Submitted by

Brandon Z. Tighe

Department of Mechanical Engineering

In partial fulfillment of the requirements

For the Degree of Master of Science

Colorado State University

Fort Collins, Colorado

Spring 2022

Master's Committee:

Advisor: Jianguo Zhao

Steve Simske
Haile Endeshaw

ABSTRACT

THE MANUFACTURING AND SOFT ROBOTIC APPLICATIONS OF FREE STROKE TWISTED AND COILED ACTUATORS

Inspired by biological systems (e.g., octopus), soft robots made from soft materials outperform traditional rigid robots in terms of safety and adaptivity because of their compliant and deformable bodies. To enable a soft robot's unique capabilities, they require a key component—the actuator. Many different actuators have been used, including the conventional pneumatic-driven and cable-driven methods, and also several emerging approaches, like dielectric elastomers, liquid crystal elastomers, and shape memory alloys. Besides existing actuation approaches, another promising actuator for soft robots is the twisted-and-coiled actuator (TCA), which can be conveniently fabricated by continuously twisting polymer fibers into a coiled spring-like shape.

In this thesis, we investigate free stroke TCAs (i.e., TCAs that can produce significant displacements without preloading). We first describe a customized machine that can automatically fabricate TCAs with free strokes by twisting a polymer fiber and then coiling the twisted fiber along a mandrel with a guide channel, which is made by wrapping a small copper wire helically about a larger one. After that, we discuss the characterization and evaluation of the fabricated TCAs. We also apply free stroke TCAs to two different soft robotic systems. The first one is a spherical tensegrity robot which resembles a tensegrity structure, a compliant yet stable structure made of rigid rods and elastic cables. By replacing the elastic cables with TCAs, we can actuate TCAs to shift the robot's center of gravity to generate rolling locomotion. The second application is a shape morphing quadrupedal robot with multiple modes of locomotion. By actively morphing the robot's body shape, we demonstrate different locomotion modes for the same robot, including walking on flat ground, crawling below a gap, and climbing across a bridge. Demonstrations for

the tensegrity robot and shape morphing robot will facilitate future biologically inspired adaptive robotic systems to actively adapt their morphologies and behaviors to different environments.

ACKNOWLEDGEMENTS

First and foremost, I would like to thank my wife, Amanda Tighe, who has believed in and supported this dream since day one. Who sacrificed countless hours of our time together and endured many sleepless nights to get us here. Who tirelessly worked to take care of me and our family so that I could focus on becoming the best engineer I could be. I want to thank my stepson, Nol, who missed out on too much family time and events this past 8 years and was often the motivation to see things through. Thanks and I love you both.

I would like to thank all of my peers throughout the years who endured this right of passage with me and likely dug me out of more than one academic hole, especially Jiefeng Sun and Haijie Zhang.

I would like to thank all of the professors who dedicate their lives to changing the world, one pupil at a time, especially: Dr. Fuji Adachi, who gave me confidence and helped me understand how a 28-year-old with a 9th-grade math education could become a mathematician and engineer. Elhadji Gaye, who was a great friend and professor. Dr. Paul Heyliger, one of the most professional, enjoyable, well-put-together professors that I ever had the pleasure of learning from. Dr. Steve Simske and Dr. Christian Puttlitz, for all of the great advice, sure, but also for taking the time and effort to council and comfort me in times of worry. I will be a happy man if I can look back on my career and see some semblance of what you guys have done. Finally, I would like to thank Dr. Jianguo Zhao, for offering me the opportunity to work in the Adaptive Robotics Laboratory, for mentoring me, and for helping me to grow as a researcher and an engineer. For over 4 years he helped to give me confidence in my strengths and to build my weaknesses stronger. Dr. Zhao always demanded and expected more than I thought I was capable of, and time and again I delivered.

I firmly believe my educational experience would be a shell of what it is today were it not for the aforementioned people and so many more. Thank you.

DEDICATION

I want to dedicate this to my mom and dad, Mike and Angela Tighe. If only you were here to see it. And to God, of course, whom I could never succeed without. And to any underdog who ever believed they weren't good enough to do something great. Let this be proof that you are.

TABLE OF CONTENTS

LIST OF TABLES

LIST OF FIGURES

Chapter 1

Introduction

1.1 Background and Previous Work

1.1.1 Soft Robotics

It has been nearly seven decades since the dawn of traditional robots, many of which have had profound contributions in areas such as material handling, manufacturing and welding, even in medicine for minimally invasive and remotely conducted surgeries. Although well developed and implemented, traditional robots have their own shortcomings and challenges. One newer subset of robotics is known as "soft robotics". Soft robots are robotic systems that are made from all or mostly compliant materials, which can be advantageous compared to their traditional non-compliant counterparts. Soft robotics attempts to mimic many of the mechanical and body systems found in nature. Having non-rigid or “compliant” components, they are generally more adaptive, flexible, and resilient, and therefore, can be more successful in harsh or unpredictable environments, as well as potentially being safer for human-robot collaboration [1]. Soft robots are less likely to undergo plastic deformation or mechanical failure due to extreme external forces because of a compliant material’s ability to hyper-elastically deform under stress [2]. Some examples of soft sensors include 2D and 3D elastomer embedded strain sensors, pneumatic deformation sensors, highly stretchable textile embedded strain sensors, and soft optical tactile sensors. Various actuators have been developed as well, such as pneumatic bending actuators, pneumatic complex bending modules that use fibers for strain limiting layers, self-healing dielectric elastomer actuators, and combustion-driven actuators.

Soft robotics have proven useful in a range of applications from rehabilitation devices [3–5] to industrial manipulators [6, 7], yet many soft robotic actuators and sensors are still in the research phase [8, 9].

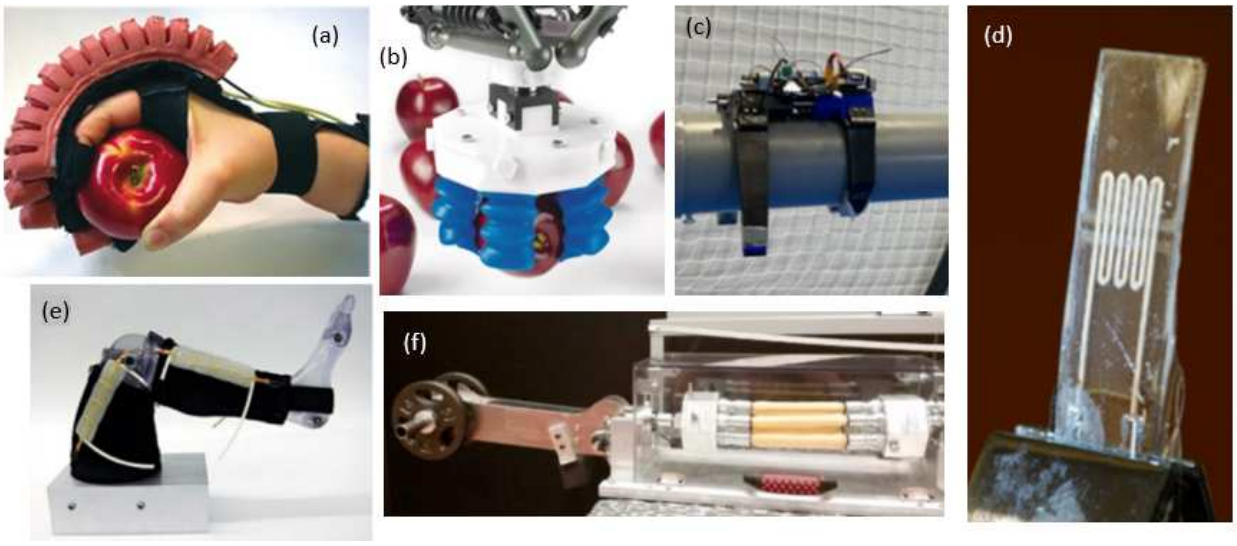

Figure 1.1: Various Soft robots. (a) A Pneu net assisted glove from Harvard [3]. (b) Industrial end-effector gripper by Soft Robotics, Inc. [6]. (c) A tentacle inspired gripper for pipe inspection [7]. (d) A compliant strain and curvature sensor [8], (e) A fiber reinforced lower extremity assisting device [10], and (f) the McKibben muscle actuated arm, currently being developed [9].

1.1.2 Artificial Muscles

As soft robotics has grown from its infancy, many different soft sensors and actuators have emerged. One class of soft actuators, labeled artificial muscles, includes a variety of different mechanisms to achieve contracting or extending linear motion. Pneumatics have been used to make simple extending and unidirectional bending [11], and have been coupled with fiber reinforcements to achieve more complex motions such as expanding, extending, contracting, bending, and twisting [12]. These actuators have the disadvantages of requiring cumbersome external pneumatic systems and complex fabrication processes. Another unique artificial muscle uses an elastomer and fluid as a dielectric and can be deformed with the application of voltage. This actuator is self-healing and can achieve high cyclic frequency, but only achieves minimal displacements and requires very high voltages to operate [13,14]. One group developed a liquid crystal elastomer (LCE) artificial muscle that has been used as an actuator in soft robotic applications [15, 16]. LCEs are programmable and actuation is reversible, but requires an external energy source and has a low cyclic frequency. One type of heat-driven artificial muscle is produced by twisting and coiling a polymer. There are many

different names and varieties of these types of actuators, but here we generally call them twisted and coiled actuators (TCAs).

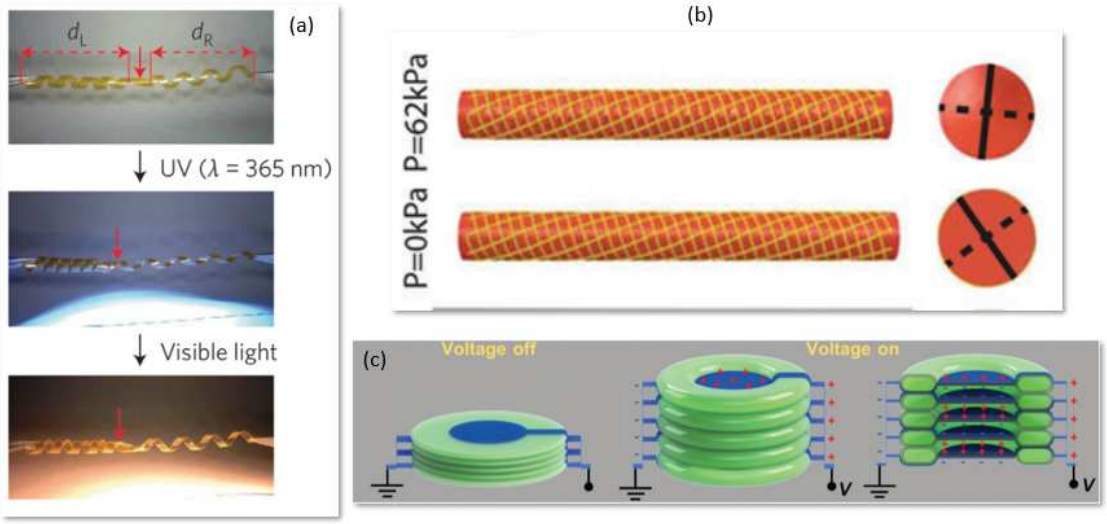

Figure 1.2: Various artificial muscles including (a) light-activated LCE muscles [16], (b) fiber reinforced pneumatic muscles [12], and (c) Dielectric elastomer DE muscles [13]

1.1.3 TCA Driven Robots

Because of their inherent advantages, TCAs are useful for many soft robot platforms. Early designs that execute 2D bending include an articulated robotic finger [17] and a simple inching crawling bot [18], the former utilizing nylon 6,6 woven thread and the latter solid nylon fishing line. Groups have gone on to create a general 3D bending module [19], a manipulator with a 3D bending arm, twisting wrist and 2D gripper [20], as well as various other bionic manipulators, arms, and wearables [21,22]. Although facing some challenges, TCAs have been used as linear actuators in two and four-bar tensegrity robots [23] [24]. Being an artificial muscle, it seems suitable that the biomedical robotics sector has seen TCAs used in projects such as a musculoskeletal system model [25], and even a mechatronic rehabilitation device [26].

1.2 Contributions

Free Stroke TCAs

To make a more useful TCA for soft robotic applications, we introduced a novel fabrication technique for contraction-type TCAs that allow for separation of the coils without preload or pre-strain conditions, which we termed free stroke TCAs. This design is ideal for applications that require antagonistically oriented muscles because, unlike their traditional counterparts, free-stroke TCAs can be embedded in soft bodies and have near-zero stress on the actuators in their natural position. The free stroke design also allows for more than a 48% contraction without a preload. Our TCAs can be arranged in different shapes and orientations within a soft body to produce large and precise programmable and repeatable motions. These TCAs could be useful in applications including intelligent structures, wearable smart textiles, haptics, and robotics [27].

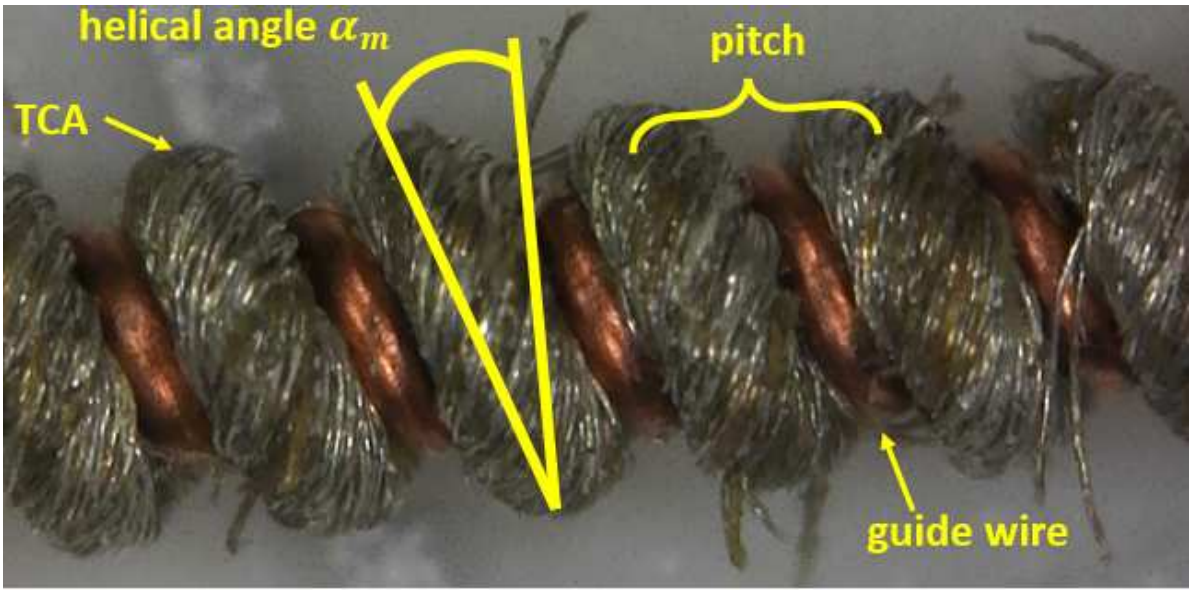

Figure 1.3: This detailed image of a TCA shows how the twisted conductive thread is wrapped around a mandrel, its coils separated by a copper guide wire.

Automated Manufacturing of TCAs

Because of the complexities involved in producing an accurate and pre-determined helical angle on our free stroke TCAs, traditional manual methods of manufacturing were not feasible. We

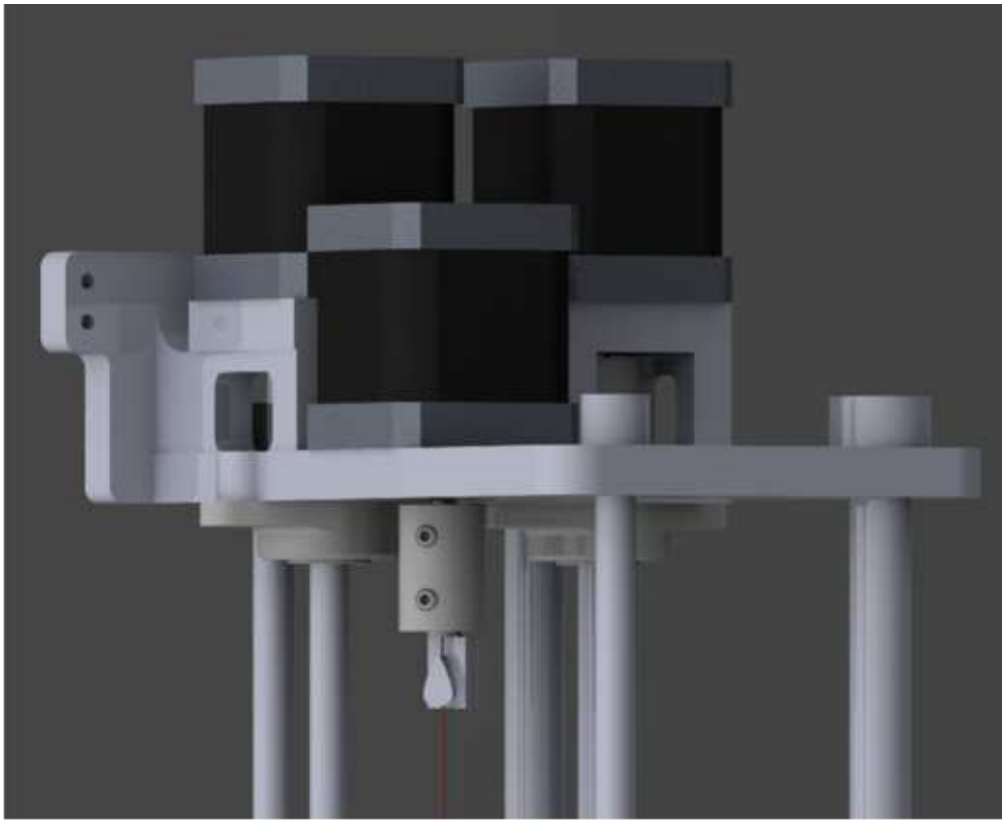

Figure 1.4: CAD model of the top portion of the five motor CNC controlled TCA manufacturing machine.

needed an automated and thus repeatable machine that could produce a variety of TCA configurations quickly and efficiently. To achieve this, we expanded on an early design of our TCA machine by making several mechanical, programming, and control improvements. A new method of twisting the thread was introduced which allowed us to use a much longer 3.8 m section of natural thread which ultimately resulted in an approximately 85cm TCA, about 6 times longer than we could produce with the previous machine. By refining the build procedure and combining some processes, we were able to make TCAs much faster and with fewer defects and irregularities. Various routines were written to allow a user to decompose the fabrication process into different parts as well as independently control motor direction and velocity which results in a more customizable, repeatable, and generally more efficient manufacturing experience.

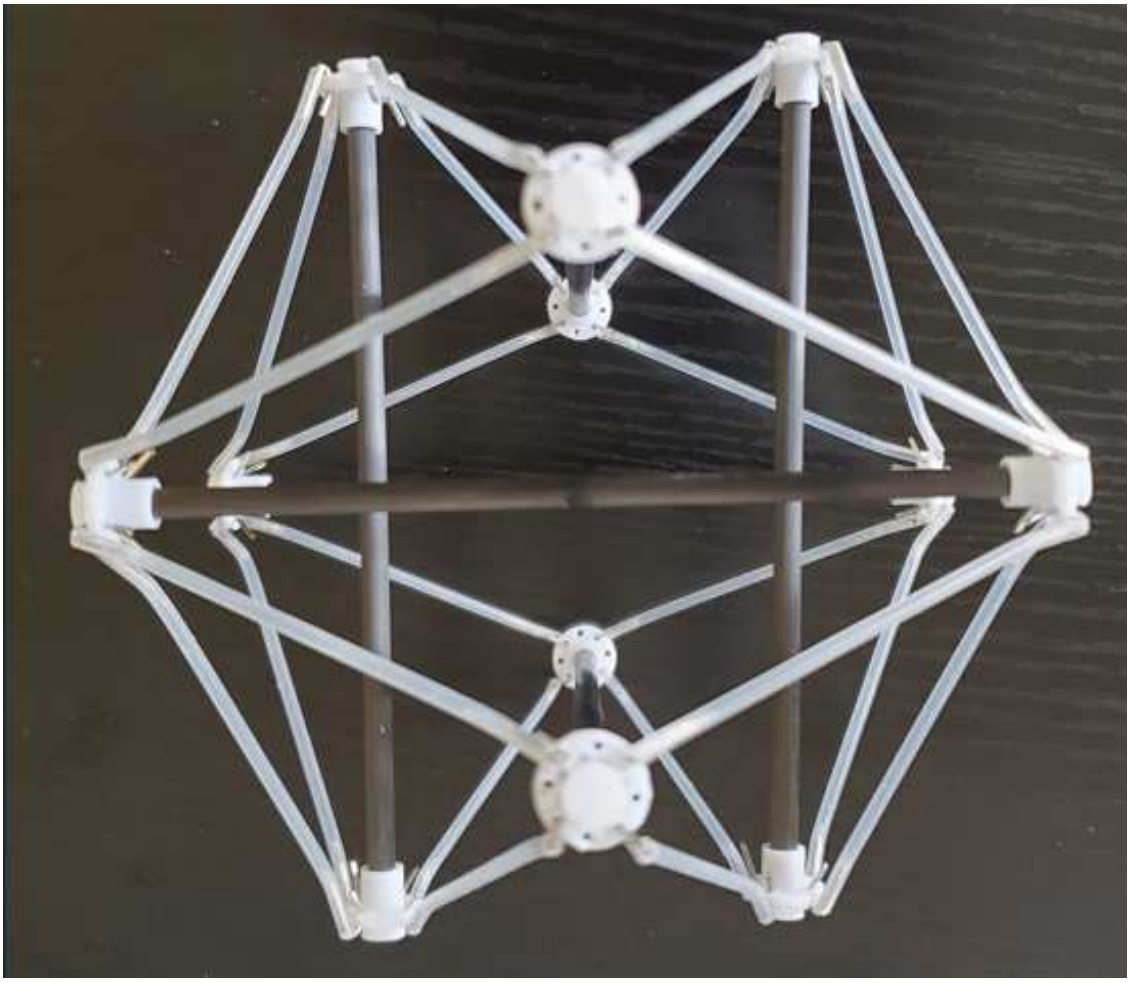

Figure 1.5: By adding artificial muscle linear actuators, we turn this six-link icosahedral tensegrity structure into a rolling robot.

Soft Robotic Application: Tensegrity Robot

One unique example of soft robotics is known as tensegrity (a portmanteau of tensional integrity) robots. This concept of rigid members in compression held together by elastic members under tension can be found in the muscular-skeletal systems of most animal species and is advantageous for four central reasons: all members are axially loaded (limited shear stress exists in the system), they can handle extreme external loading and impact shocks, they are deployable, and they have an extremely high weight to load capacity ratio. Some relatively well-refined large-scale spherical tensegrity robots exist, but current actuation methods prevent scaling down the products successfully due to limitations in available components, and complex mechanical and sensory sys-

tems. In this project, we used TCA soft actuators (which double as strain sensors) to actuate a six-link icosahedron tensegrity robot and were able to successfully realize three unique step types which could theoretically be chained together to realize rolling locomotion from any possible starting condition.

Robotic Application: Shape Morphing Robot

Figure 1.6: The fully assembled modular, multimodal shape morphing robot.

The goal of this project was to make a quadrupedal robot that was capable of altering its mechanical structure in order to realize various modes of locomotion. This is a significant shift towards replicating animalia movements which is more complex and useful than traditional robot

locomotion which is typically limited to only one mode of locomotion. The primary components of this robot are four 3D bending modules acting as legs and three shape morphing modules oriented in parallel and acting as the robot body. Both the 3D bending modules and shape morphing modules are driven by TCAs. The project in large was successful as we were able to morph the robot body into three different configurations allowing us to realize a crawling gait, a walking gait, and a climbing gait.

Chapter 2

The Manufacturing of Twisted and Coiled Actuators

2.1 Working Principles of TCA

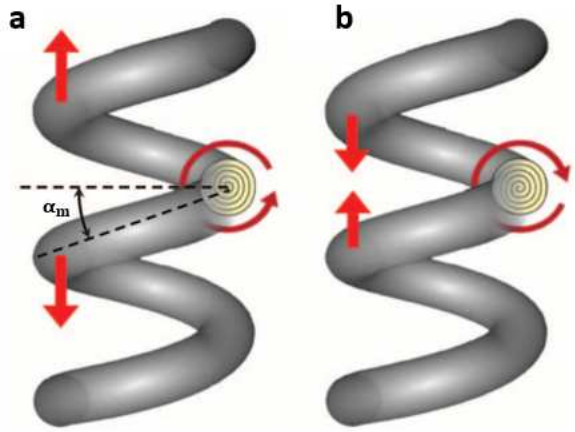

Figure 2.1: Illustration of the working principles of a TCA. (a) heterochiral twisting of the fiber produces an expanding muscle, whereas (b) homichirally twisted fibers cause the actuator to contract when thermally activated. The helical angle of the coiled thread is denoted helical angle (α_m) [28].

TCAs take advantage of the anisotropic heat expansion derived from polymers when their chains are oriented in a specific fashion. Twisting a strand of nylon (Figure 2.1a), for instance, will align its polymer chains in such a way that when heat is introduced (Figure 2.1c) the material will expand and contract, promoting untwisting of the fiber. The amount of expansion in itself is not very useful, but if the twisted thread is oriented in a "spring-like" fashion by coiling around a mandrel (Figure 2.1b), it will produce usable displacement. Nylon 6,6 is an ideal polymer for this application because of its high softening point, toughness, and thermal expansion ratio [17]. As a twisted strand of the polymer is heated, it simultaneously expands along the radial direction and contracts along the axial direction, both of which contribute to the fiber untwisting. The amount of axial contraction that occurs is negligible and not very useful. However, the torsional actuation force produced during this process can be exploited to attain large linear displacements when the

fibers are formed into a helical orientation. If the twisted fiber is coiled in a homochiral manner (Figure 2.1a), that is, coiled in the same direction as the twist, then heat expansion of the material will result in an axial contraction of the coil. On the other hand, if the twisted fiber is coiled in a heterochiral manner (Figure 2.1b), then the coil will expand axially upon heating. A contracting TCA can usually contract until the gaps between the coils close and the coils contact each other.

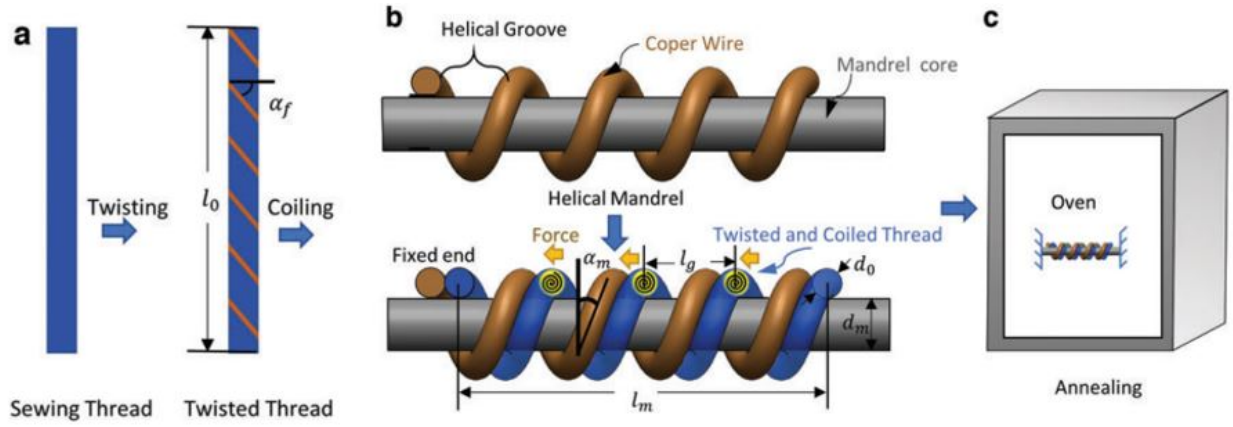

Figure 2.2: TCA Fabrication Setup and Parameters, including (a) applying twist to the natural conductive nylon thread, (b) fixing the copper guide wire to the mandrel core before coiling twisted thread, and (c) the oven annealing process with the ends of the TCA fixed to prevent uncoiling.

A *free stroke* TCA is designed so that an unloaded TCA can produce a significant stroke. The gap size is a function of the made helical angle (α_m), which can be adjusted to tune for the desired stroke length and actuation force. Furthermore, other characteristics of a TCA can be tuned by adjusting parameters such as the amount of twist inserted into the natural thread, the twisted fiber diameter, the coil diameter, and the annealing temperature.

2.2 Automated Manufacturing of TCAs

2.2.1 Manufacturing Other Twisted Actuators

The general procedure for fabricating conventional TCAs is to twist a polymer strand until it begins to coil on itself, ideally until the entire length has coiled on itself one time. Suspending a

mass from the coiling TCA prevents it from over-coiling. The coiled TCA must then be annealed to reorient the polymer strands and allow the TCA to maintain its shape.

There are many different materials and methods of making twisted and coiled actuators as well as many different names they go by. Twisted Artificial Muscles (TAMs) [29] are produced by self-coiling 0.5mm nylon 6,6 fiber and 0.1mm enameled copper wire as a heating element. This rudimentary self-coiling method of making twisted actuators is the most common and involves twisting the polymer and heating element together by using a motor on the top of the strands and suspending a mass from the bottom. It is also important to have a mechanism in place to prevent the lower portion from spinning. After a certain amount of twist is put into the strands they will begin to coil on themselves until eventually, the entire length is twisted and coiled. This manual method of producing twisted actuators oftentimes results in manufacturing defects such as over-coiling or uneven distribution of coils across sections of the muscle.

Twisted and Coiled Polymers (TCPs) [30] which have been used in soft robots [31] and wearable haptic feedback devices [22] are produced using 0.2mm braided UHMWPE, a NiCr heating element and a similar self-coiling method as described above. They are then annealed by adding a voltage to the NiCr wire in four 5 minute intervals. This particular TCP is capable of achieving a 5.2% contraction when heated to its maximum non-destructive temperature of approximately 110C.

One group has been making twisted actuators with conductive nylon thread twisted with several strands of spandex, which they dubbed STCAs. The addition of spandex allows the artificial muscle to attain a pre-stretch of 230%, which is much more than most designs. In this method, eight strands of pre-stretched spandex and one strand of size 92 (0.337mm) conductive nylon thread are set to a fixed length and twisted through three stages until a sufficient amount of twist is introduced into the muscle. The bottom of the muscle is then attached to a slider which allows for axial movement but not untwisting and the muscle undergoes two more stages of twisting which promotes the strands to self-coil. Unlike the previous designs, STCAs must undergo 2 stages of self-coiling but can achieve more than 10% contraction. The authors developed a simple machine

to produce six STCAs simultaneously. STCAs have been made with a single helix coil [32] as well as a double helix design [33]. Although they built a machine for fabrication, the process is not automated, the design of twisted actuators is not tunable and oftentimes requires post-processing after annealing. Since the muscles tend to over coil three or four times, a fabricator must manually remove the extra coils before use.

One research group [34] produced Coiled Polymer Actuators (CPAs) using 50lb nylon fishing line and Nichrome 80 resistive wire, the researchers developed a machine to improve upon the common method of producing self-coiling twisted actuators (i.e. a motor on top, suspending a mass from the fiber and manually twisting), by designing two separate devices, one to prepare specific length pre-stretched nylon strands and another to hold the strands and heating element under constant tension while inducing twist. The devices were proven to improve the performance and repeatability of the actuators but fell short in their lack of adjustability, control, and the varieties of twisted actuators they can produce.

2.2.2 Design of Our Customized Machine for Various TCAs

Conventional TCAs have little to no stroke length unless they are preloaded with enough force to stretch them out. These forces are a hindrance for soft robotic applications as many of the hyper-elastic materials used will deform under them. However, if a TCA can be built and annealed with a predetermined helical angle, then it would be able to produce a useful stroke without requiring the pre-stressed conditions. This can be achieved by coiling a twisted polymer around a mandrel with a helical guide on it. Fixing both ends of the twisted fiber to the mandrel will prevent it from uncoiling before and during the annealing process. To ensure consistent contraction or expansion along the length of a TCA, certain parameters must remain constant during the fabrication process, such as twist distribution, helical angle, and coil diameter.

Design Considerations

We needed a machine that could not only produce high-quality TCAs with minimal manufacturing discrepancies and defects but was also capable of making a variety of TCAs through

alteration of helical angle, adjustable pre-twist, the capability to use various diameter and material mandrels. We also wanted our machine to be easy to learn and use, safe to operate, and robustly built for longevity. Being able to make longer continuous sections of TCA (>20cm) allows for a wider range of applications and minimized the variation in performance that results from manufacturing discrepancies. There are some specific steps required for making our free stroke TCAs which we categorized into 6 specific processes: Preparing the raw materials, wrapping the guide wire onto the mandrel, twisting the conductive nylon thread, coiling the twisted thread onto the mandrel, annealing the TCA, removing the guide wire from the TCA. We wanted to design our TCA machine to conduct each process, except for the annealing and preparation of raw materials.

To accurately twist to the natural thread, our machine required stepper motors controlled by a sub-routine that executes a predetermined amount of rotational displacement. During twisting, the thread must be subjected to enough axial tension to prevent it from coiling onto itself. Instead of fixing one end of the thread and twisting the other, we used two motors and a weighted pulley to twist the thread in a "doubled back" orientation, which cut the twisting time in half and allowed us to start with twice the length of natural thread we could otherwise use. To accurately control the helical angle of the guide wire (and thus TCA), we used lead screws and linear shafts to synchronize the mandrel spinning with the linear motion of an axially traveling guide (which maintains a consistent helical angle).

Mechanical Design

We leveraged some clever design ideas to simplify the machine and maximize its efficiency. For example, by using certain motors for more than one purpose we could consolidate our two previous machines into one. By logically ordering the manufacturing process, we eliminated previously problematic fabrication steps, and by using a "doubled back" thread twisting configuration we were able to make TCAs with a 3.8m natural thread length, resulting in 80cm final TCAs.

The first process in building a TCA is wrapping the guide wire around the mandrel. This is done by simultaneously turning the mandrel about its axis and using a traveling wire guide to control guide wire placement. To accomplish turning the mandrel we placed two opposing,

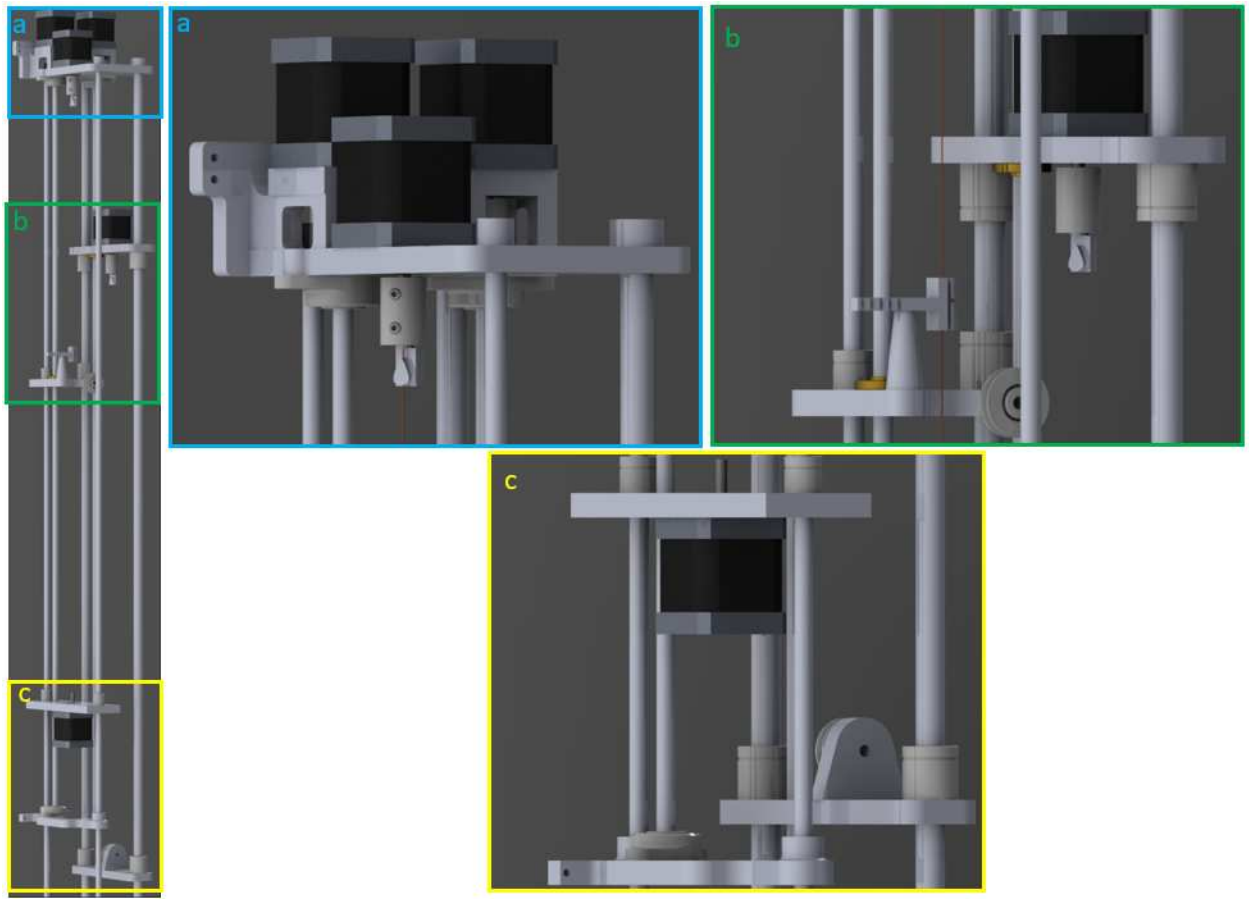

Figure 2.3: Detailed views of the TCA machine. (a) The upper assembly (b). The traveling motor and guide. (c) The lower motor and switchback pulley.

synchronized NEMA 17 stepper motors (motors 1 and 3; all motor designations will be referenced from Figure 2.5) one meter apart. We did this by fixing the top motor (1) to the machine frame and mounting the lower motor (3) to a plate attached by bearings to two 8mm x 1m linear motion rods, which enables a user to make various length TCAs (between 20 cm and 80 cm). Adding masses to the traveling lower motor mount plate enables the operator to maintain constant tension on the mandrel. The guide-wire traveling guide was mounted to a plate attached to two linear motion rails and its position was controlled using a 1m long T8, 2mm pitch lead screw which was rotated by motor (4) thas was fixed to the top of the machine frame. The wire guide itself is easily changeable and specific to the mandrel diameter being used. It was built on a pivoting axis which allows the operator to use silicone tubes to adjust the amount of force with which the guide is pressed against the mandrel.

The next operation is to twist the natural (untwisted) thread, which is difficult as the length of natural thread needed is approximately 4 times the final length of the TCA and it must remain under a specific constant tension to prevent it from self-coiling. To maximize the length of natural thread we could use, we built our TCA machine 2m tall and used a doubled-over method to maintain tension. We connected the thread to two downward-facing motors (4,5) at the top of the machine and ran it through a pulley that is mounted on a sliding plate that freely moves axially along two 12mm x 2m linear guide rods. To use motor (4) for wrapping the guide wire on the mandrel and twisting the thread, we needed to place a hook on the plate next to the motor to temporarily hold the top end of the prepared mandrel while twisting the thread. In order to tune the tension of the twisting thread, masses can be attached to the free-floating sliding pulley plate.

The next process, coiling the twisted thread onto the prepared mandrel, involves keeping the twisted thread under constant tension and using the traveling guide to seat it in the valley created by the guide wire. Similar to the mandrel wrapping process, motors (1,3) turn the mandrel while motor (4) moves the guide consistently along the length of the mandrel. Additionally, motor (5), which is parallel to and slightly offset from motor (4), drives another t8 lead screw that moves the mounting plate for motor (2) vertically in sync with the traveling guide. The purpose for this is twofold: lowering the "bottom" side of the twisted thread allows the end of it to essentially meet the TCA at the bottom of the mandrel, minimizing wasted material, and secondly, it helps to transfer the twist of the thread through the pulley, ensuring an even twist distribution across the length of the TCA. Further, motor (5) slowly untwists the thread to compensate for the additional twist that accumulates on the lower end of the twisted thread.

Electrical Design

The mechatronic portion of the machine consists of the five aforementioned NEMA-17 stepper motors which are controlled using an Arduino Mega microcontroller outfitted with an open-source 3D printer motor controller known as the RepRap Arduino Mega Pololu Shield (RAMPS) specifically version 1.4 as it was expanded to simultaneously control 5 motors (see Figure 2.4 for wiring diagram). To adapt the 3D printing controller for our use, we altered an open-source library "Ac-

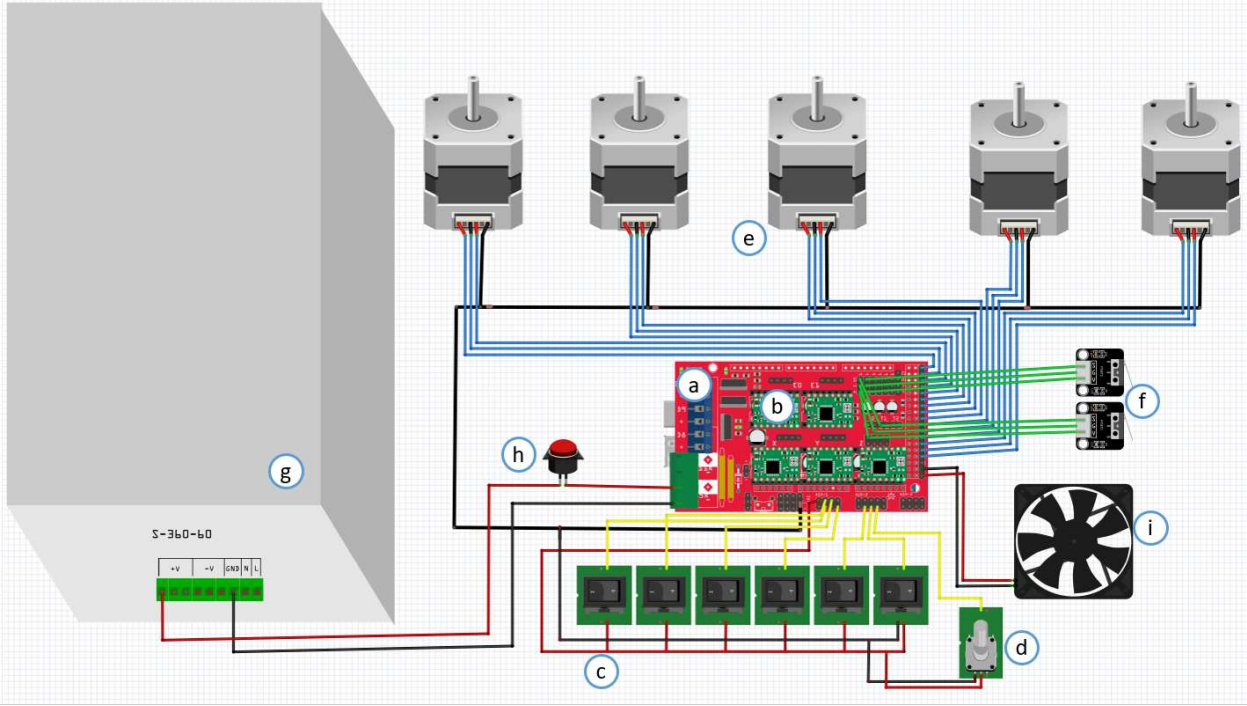

Figure 2.4: Diagram showing the microcontroller and electronic components of the TCA manufacturing machine. (a) A RAMPS shield is mounted onto an Arduino Mega microcontroller, (b) Pololu DRV8835 motor drivers supply current to the NEMA 17 stepper motors. LED rocker switches (c) and a potentiometer (d) are used to select the machine function and control the motor speed, respectively. Limit switches (f) prevent the linear motion components from over travel. Power is supplied to the system using a 24V power supply. An emergency stop button (h) is connected into the circuit and the control package is cooled using a 30mm fan (i).

celStepper.h", which allowed us to gain independent control of the motors. Each motor required three pins, one to send the step signal, an "enable" pin used for controlling speed, and a "phase" pin to control the motor direction, as well as being attached to the common ground. In this instance, digital pins are sufficient. Motor one used pins 26, 28, 24, motor 2 used pins 46, 48, 62, motor 3 used pins 36, 34, 30, motor 4 used pins 54, 55, 38, motor 5 used pins 60, 61, 56 (listed as step signal, phase and enable, respectively). Mechanical stops or "limit switches" were added on either side of the lead screws to prevent accidental over traveling of linear motion components and were connected to the Arduino's VCC for power, signal pins 2 and 3, and the common ground. We 3D printed a case for the control package of the machine that housed the microcontroller and provided a user interface. An emergency stop button was installed in serial between the 24V 15A power supply and the Arduino. Six led lighted rocker switches were wired into the microcontrollers 5V

pin, common ground, and digital in pins, one for each of five operations: twist the thread (pin 42), coil around the mandrel(pin 44), move motor 2 (pin 57), turn mandrel only(pin 58), home travelers(pin 63), and one to reverse any operation(pin 40). Any signal from one of these buttons triggers a for-loop with a sub-routine for each operation. A potentiometer designated for selecting speeds was attached to the board's 5V rail, common ground, and analog input pin A0. To avoid compound errors that arose from having a wide range of speeds available, the potentiometers input reading was partitioned into 5 categories ranging from low to high, each with a corresponding maximum speed coefficient. Finally, a 30 mm cooling fan was attached to the Arduino power and ground so that it would be on any time the machine is in use. The helical angle α_m for the TCA is a function of the mandrel diameter and its rotational velocity and the translational velocity of the guide as seen in the following equation,

$$\alpha_m = atan(V_t/2\pi d_m V_r) \tag{2.1}$$

where V_t is the traveling guide's translational velocity, d_m is the mandrel diameter, and V_r is the mandrel's rotational velocity. A variable "traveler guide speed" can be adjusted in the Arduino code to change the rotational/translational speed ratio to specify a TCA's helical angle. Further, the amount of twist put into the thread can be set for a given length according to the ratio of 600 twists/m of natural thread.

Machine Operation and TCA Fabrication

For the specific configuration of TCA that we used in the soft robotic application portion of this work, 26 ga copper wire was selected for the mandrel core, 32 ga copper wire for the guide wire, and 235/36 dtex 4 ply conductive wire thread (V Technical Textiles, Inc. PN200121235364HCB). The TCA machine was set to produce a (15.57°) helical angle. The manufacturing of a TCA can be split into five separate processes: building the mandrel, twisting the thread, coiling the twisted thread around the mandrel, annealing the TCA, and finally removing the guide wire from the TCA, each of which I will explain in detail.

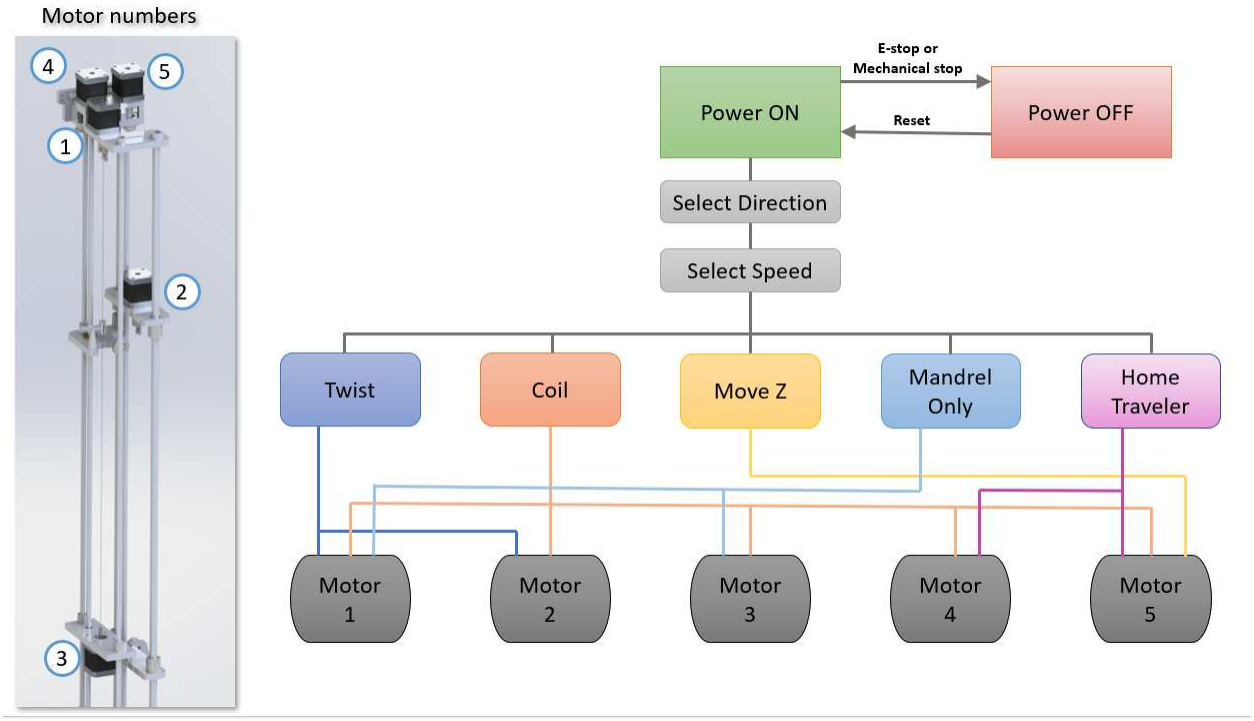

Figure 2.5: Model labeling each of 5 motors on the TCA machine (left) and a schematic showing which motors are used for each operation (right).

To make the mandrel, we start by cutting a 90cm section of 26 ga copper wire and twisting approximately 1cm diameter loops on both ends. Connect the mandrel to motors (1) and (3). Twist a loop into the free end of the 32 ga wire, attach it to the same side hook as the mandrel and unwind approximately 2.5m from the spool. After running the guide wire through the lower pulley and back up towards the top of the machine, clamp the spool to the traveling plate that motor (2) is mounted to in a fashion so that it will not unspool more wire. Ensure 500 g mass is added to the plate that the pulley is mounted on to apply appropriate guide wire tension. With the speed selection set to medium, use the "mandrel only" function to secure the guide wire to the mandrel and position it to insert into the traveling wire guide. With the guide wire seated into the traveling guide and tensioner rubber bands on, increase the motor velocity to high and use the "coil" function to coil the guide wire around the mandrel. Make sure to closely monitor the machine and manually stop at the bottom of the TCA (before triggering the lower limit switch). Reduce the motor speed to medium and use the "mandrel only" function to secure the guide wire at the bottom of the mandrel,

being careful not to relieve tension as that can cause an erroneous and nonuniform helical angle. After securing the guide wire, terminate it by cutting and tying off the excess.

Next, we will free motor (1) for the next operation by removing the mandrel from the motor and placing it on the hook beside motor (1). With the motor speed set to high, use the "home travelers" function to bring motor (2) and the traveling guide back to their starting positions. The next process is to prepare and twist the thread. To make an 80cm TCA, cut 3.6m of conductive thread and tie small loops on both ends. Attach one end to motor (1) and after running the thread through the lower pulley, attach the other end to motor (2) and make sure the 500g mass is on the lower pulley plate and that the thread is under tension. It is important to ensure that the machine is set to apply the appropriate amount of twist for the chosen length of natural thread as discussed in the previous section. After doing so, ensure the motor speed is set to high and use the "twist" function to begin twisting the thread. The machine will automatically stop when the appropriate amount of twist is inserted into the thread.

To coil the now twisted thread around the mandrel, remove the mandrel from the hook and attach it to the motor on the opposite side as the thread loop. Use medium or low speed and the "mandrel only" function to secure the thread to the mandrel, place it into the traveling guide, and align it with the guide wire that was previously attached to the mandrel. On the high-speed setting, use the "coil" function to coil the twisted thread onto the entire length of TCA. Once completed, twist a loop in the mandrel at the top and bottom before removing it from the machine, so that the tread cannot untwist or uncoil from the mandrel.

Next is the annealing process, which is also dependent on the materials used and the configuration of the TCA being built. For our purposes, anneal in an oven for 2 hours at 185°C. Finally, after the TCA has cooled off we can remove the guide wire. This is done by untwisting the "locking loops" from the mandrel and replacing it back onto motors (1) and (3). Next, cut the guide wire and hold the end with pliers or by hand while using the "mandrel only" function to unwind the guide wire. The TCA is now ready for use or storage. Typically we leave the TCA on the mandrel core while storing it to prevent deformation due to viscoelastic creep.

2.3 Results and Characterization

2.3.1 Results

When ready for use, the TCA is cut to the desired length then removed from the mandrel, terminated, and placed in a circuit with a power source. As the TCAs use a relatively low amount of power, we can generally use a 2 A motor driver controlled with Pulse Width Modulation (PWM) via a microcontroller. To remove any internal stresses from the manufacturing process and ensure consistent performance, the TCAs must be "trained". This is done by applying a low (<1 A) current for short bursts (1 s) for 10-20 cycles.

To compare the performance of our free stroke TCAs with conventional TCAs (that is, without gaps between neighboring coils), we made several variations adjusting two parameters: initial helical angle of the TCA (a_m, Figure 2.2b) which influences the potential displacement, and annealing temperature T_a which influences the actuator's dynamic response. The maximum displacement for a TCA can be described as a function of the initial gap between coils of a TCA (l_g, Figure 2.2b) with the following equation

$$\delta_l = n(l_g - d_0) \tag{2.2}$$

where δ_l is the displacement, n is the number of coils, d_0 is the initial diameter of the twisted thread, and l_g is the distance between TCA coils, which can be related to helical angle α_m according to the relationship

$$l_g = 2tan(\alpha_m)(d_m + d_0) \tag{2.3}$$

where d_m is the diameter of the mandrel's core and d_0 is the diameter of the twisted thread. We chose to alter these fabrication parameters to add to the bodies of work that have already been done to characterize the effect of spring index, amount of twist applied, number of plies in the thread, and the use of different polymers [28, 35]. Of the four free stroke TCAs built, two were classified as Type 1 and two as Type 2, which had helical angles of 15.57°and 22.54°, respectively. Further, we annealed one of each type of TCA at 180°C and the other at 200°C. The naming convention

used here lists the type of TCA followed by the annealing temperature. For example, a Type 1-180 TCA has α_m= 15.57 and was annealed at $T_a = 180$°C.

All of the free stroke TCAs have initial gaps between coils, that is $l_g > 0$. With no load applied and at room temperature, the TCAs have an initial or *natural length* l_n. When heated, the TCA contracts until the coils are all touching (l_g =0), which is denoted as the minimum length or l_min and upon returning to room temperature a TCAs length returns to l_n. Using these principles the *free stroke* S_f of a TCA can be calculated similarly to strain in engineering mechanics.

$$S_f = (l_n - l_{min})/l_n \tag{2.4}$$

To demonstrate the free stroke actuation of our TCAs under no initial strain, we pulled a mass horizontally across a vinyl sheet. Our experimentation showed that our Type 2-200 actuator with a mass of 0.03 g was able to overcome a frictional force of approximately 0.4 N for a stroke length of S_f=48%. Further, we were able to connect five Type 2-200 TCAs in parallel (weighing 0.16 g) and drag a 2 kg mass 60 mm. By fixing a natural length TCA at both ends, we determined that a single actuator could produce 0.78 N force before catastrophic failure.

Our free stroke TCAs can also work under an initial load similar to traditional TCAs. TCA stroke with a pre-load is defined as

$$S = (l_{load} - l_{min})/l_{load} \tag{2.5}$$

where l_{load} is the final length when the weight of the load and the TCAs spring force reach equilibrium. Test results showed that our Type 2-200 TCA could produce a 55% stroke under a 10 g load.

2.3.2 Free Stroke TCA Characterization

We experimentally characterized our free stroke TCAs through two separate pathways. First, we experimentally determined the static response with respect to temperature so that we could

compare it with various other groups' traditional TCAs. Secondly, we experimentally evaluated the dynamic response for four different free stroke TCAs (Type 1-180, Type 1-200, Type 2-180, Type 2-200).

To illustrate the improved static response with respect to temperature, we fabricated traditional type TCAs by coiling twisted thread around a mandrel with no gaps between the coils. We annealed it at 180°C and thus labeled it Type 0-180. We used the same thread and fabrication parameters to make Type 1-180 TCAs for comparison. To perform the static response experiment we made three of the same length for each type of TCA. Because the fabrication process has been automated, discrepancies between samples were minimal. Each sample was mounted inside an oven with a mass hanging from it and the temperature was slowly increased while the TCA displacement was recorded. We then determined the mean values of displacement with the standard deviation for each experiment. The maximum standard deviation was determined to be 2.14mm, seen in Figure 2.6a-c.

We plotted the experimental results for displacement with respect to temperature Figure 2.6a using three different initial loading conditions by suspending 0 g, 20 g, 40 g masses. The plots show nearly overlapping curves during the initial lower temperatures (>70°C), which indicates similar behavior among configurations. Eventually, each curve begins to level out which is a consequence of the coils touching and leaving no space for further displacement. A comparison of the different types of TCAs with the same weight shows that our Type 1 TCA generated larger displacements across the board. Further, as the preload mass increased so did the difference in maximum displacements. In detail, for the 0 g preload condition, over a (25°C to 150°C temperature range, the Type 0 TCA contracted 4mm, whereas the Type 1 produced 20 mm of contraction. It is worth noting that since a traditional TCA has almost no gaps between coils, most of the 4 mm of displacement was from the TCA curling up onto itself. With the 40 g masses (and 25°C to 150°C temperature), the Type 0 TCA produced 24 mm of contraction and the Type 1 TCA was able to achieve 44 mm of displacement. It is clear to see that traditional TCAs can only achieve useful displacements while under preloaded conditions.

We can use a mathematical model to better understand the difference in performance between free stroke TCAs and traditional TCAs. The relationship between temperature and displacement can be defined:

$$F = k(l - l_n) + c\triangle T \tag{2.6}$$

where F is the preload force, k is the TCA stiffness coefficient, c is the force-temperature coefficient, l is the TCA length and $\triangle T = T - T_0$ is the change of temperature (with T being the final temperature and T_0 the initial temperature.)

By rearranging the previous equation, we can get the relationship between TCA length and temperature:

$$l = -\lambda\triangle T + l'_n, l_{min} \leq l \tag{2.7}$$

where $\lambda = c/k$, $l'_n(m) = F/k + l_n = mg/k + l_n$, and of course m and g are mass and the gravitational coefficient, respectively. This relationship is useful for illustrating the difference between free stroke and traditional TCAs in two separate instances. First when F=0, traditional TCAs cannot contract since $l'_n = l_n \approx l_{min}$. Whereas with free stroke TCAs, $l'_n = l_n \geq l_{min}$, a free stroke contraction is possible until it reaches l_{min}. To illustrate this behavior, we plotted the length with respect to temperature for both TCAs and labeled the l_n and l_{min} as seen in Figure 2.6b and c. Also, the blue shaded areas represent free stroke and show the large difference between conventional and free stroke TCAs. Second, for a fixed weight ($F > 0$), $l'_n(m) = F/k + l_n$ will be greater for a free stroke TCA because its value for k will be smaller under the same manufacturing conditions. In this scenario, free stroke TCAs can achieve larger displacements as indicated by the different weight curves in Figure 2.6b and c. The dash-dotted lines represent an approximated λ (polynomial approximation $\lambda = a\triangle T + b$) and they match closely to experimental results.

The plot of the static response of free stroke TCAs with respect to temperature shows the relationship between helical angle and actuator displacement. Another characterization we performed was to determine how annealing temperature affects a TCAs dynamic performance. Aside from a free stroke, this is very important in the field of soft robotics to improve the slow actuation rate

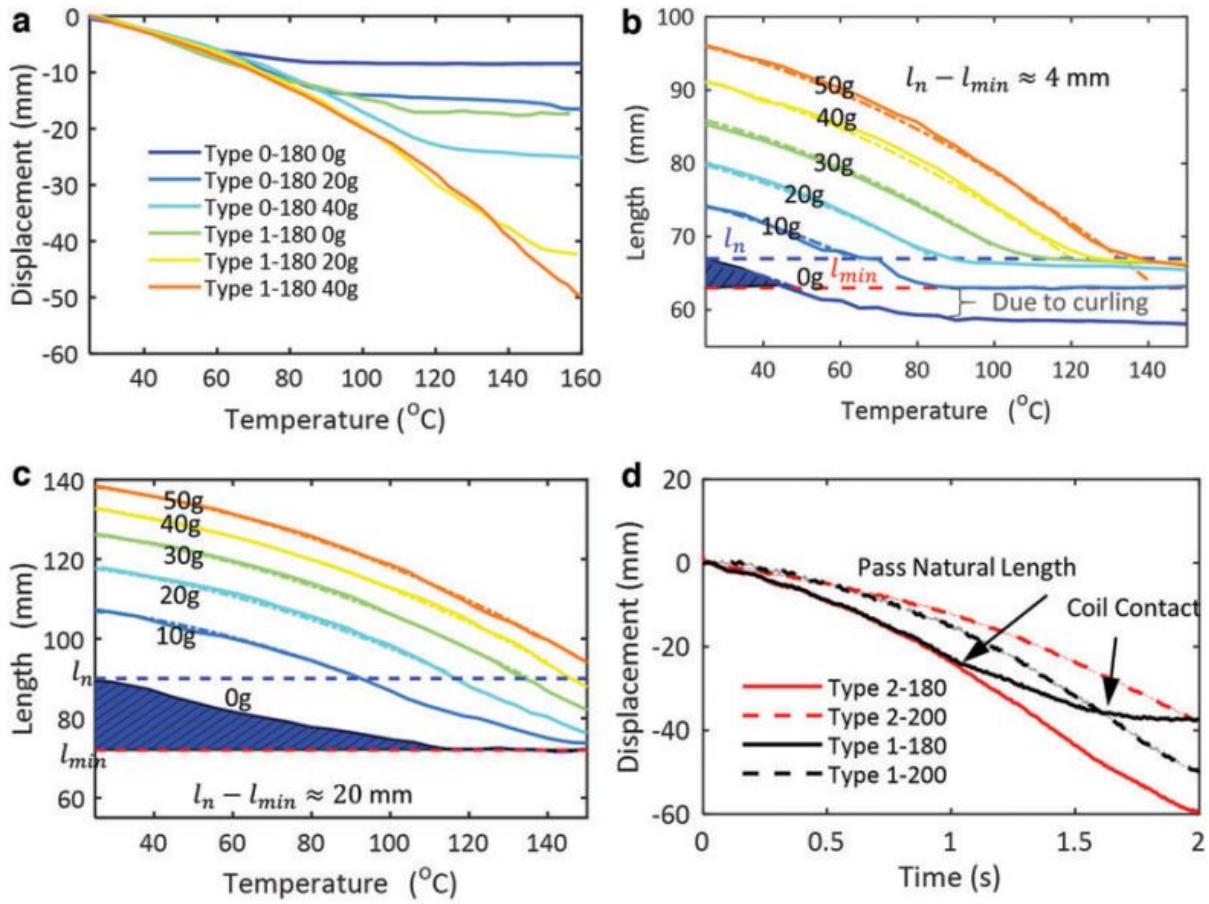

Figure 2.6: Characterization data of helical angle and annealing temperatures effects on the static and dynamic responses of TCA. (a)Displacement with respect to temperature for Type 0-180 and Type 1-180 TCAs under different loading conditions. (b) The fitted (*dash-dotted lines*) and experimental (*solid lines*) of conventional (Type 0) TCA length with respect to temperature. (c) The fitted (*dash-dotted lines*) and experimental (*solid lines*) of our free stroke (Type 1) TCA length with respect to temperature.(d)The dynamic response with respect to time for four different free stroke TCAs, each with 1A current and a 20 g load. The maximum standard deviation is 2.12.

of most TCA-driven soft robots. Some examples are a soft bending module that requires 10 s of actuation to bend 60° [19] and a crawling robot that moves 1.2% body length per second [18], both very slow compared to a shape memory alloy actuated crawling robot that can locomote at speeds of over 200% its body length per second [36]. The made length l_m of a TCA is a function of the length of the twisted thread l_0 as seen in Figure 2.2 (a). The made length of a TCA after annealing and removing the mandrel is approximately $l_m = l_0 \sin \alpha_m$. Generally the natural length $ln \leq l_m$ depends on the annealing temperature T_a.

If the annealing temperature T_a is below the TCA material's Brill transition temperature (160°C for Nylon 6,6), then the TCA will not hold its helical angle. The gaps between coils will close and the TCA will have a short natural (not loaded) length. This can happen quickly if the TCA is subjected to heat for a few cycles, or without being actuated, it can happen slowly over the course of multiple days through a process called viscoelastic creep [37]. Also for nylon, if 160°C < T_a< 200°C, then after removing the mandrel, the TCA will creep to a length between the minimal length and the made length. Specifically, the natural length of a Type 1-180 TCA is 92.5% of its made length and the natural length of a Type 2-180 TCA is 80.5% of its made length. This happens with lower annealing temperatures because the annealing process does not fully remove internal stresses in the TCA. When a Nylon 6,6 TCA is annealed at higher temperatures (T_a=200°C), it nearly holds its made length, meaning that a TCA's natural length is a consequence of both helical angle and annealing temperature.

To experimentally characterize their dynamic response, each of the 4 TCAs were fixed at the top and loaded with a 20 g weight. We then applied 1 A current for 2 s. As the TCAs were all made with the same natural length conductive thread, each had a similar resistance and temperature increase. Displacement with respect to time was plotted for each TCA Figure 2.6d. The maximum standard deviation for the four curves was 2.12 mm, which was less than 4% of the maximum displacement. The experimental data collected indicate that a TCA with T_a= 200°C will have a larger natural length (and therefore can produce larger displacements) but has a slower time response compared to a TCA annealed at 180°C. In other words, a nylon TCA annealed at 180°C can generate faster motion than its 200°C counterpart. Comparing both TCAs with T_a= 180°C, we saw that the Type 1-180 actuation speed drops at a certain point and its final displacement after 2 s heating was less than that of the Type 2-180, simply because a Type 1 TCA has a shorter natural length and so produces less displacement. We determined that a Type 2-180 TCA is a good candidate for actuating soft robots as they produce the most displacement with the fastest actuation speed.

Notably, we observed a *temporary natural length* as a consequence of Nylon's viscoelastic creep, which coincides with previous research done by other groups [38, 39]. When a load is suspended from a TCA, it initially acts like a spring due to its helical structure and seems to settle on an equilibrium length, but will actually gradually increase over the course of hours. Once the load is removed, the TCA will begin to return to its natural length at room temperature, but again is a relatively slow process. To avoid the deformation caused by unwanted forces from a TCA embedded into an elastic body, we conduct a heating cycle before embedding the actuator. We tested the life cycle and results of "aging" on a TCA by actuating a Type 1-180 TCA 10,000 times (0.25 Hz, 2 MPa load) and found that the stroke changed by only 2%.

2.3.3 Conclusion

The working characteristics of free-stroke TCAs are notably better than conventional TCAs for soft robotic applications because they do not require pre-loading to produce substantial displacements. Our automated TCA fabrication machine worked flawlessly to produce consistent, custom TCAs with a variety of different helical angles, pre-twist conditions, spring indices, and lengths.

We conducted characterization experiments, which included testing a TCAs dynamic response with respect to time static response with respect to temperature. The conclusion of this characterization suggested that TCAs made with a relatively high pitch angle, that are annealed at lower temperatures will produce a faster, longer stroke.

Future work for TCAs may include leveraging their built-in self-sensing capabilities for closed-loop control. We may also work on using TCAs to make soft-bodied, underwater robots as the heat transferred from an underwater TCA is much more efficient.

Chapter 3

Soft Robot Application: Spherical Tensegrity Robot

3.1 Introduction

A six-link icosahedron tensegrity robot design has been the basis for multiple research and engineering projects over the past decade, most of which are large-scale (>1m), use traditional rigid robotic components, and have various disadvantages such as having an inefficient energy transfer, being slow to actuate and locomote, not being easily scalable, and not being fully self-contained. This project explores the viability of coupling soft-robotic artificial muscle actuators with the tensegrity design to make a small scale (<10cm), spherical rolling tensegrity robot that addresses these shortcomings.

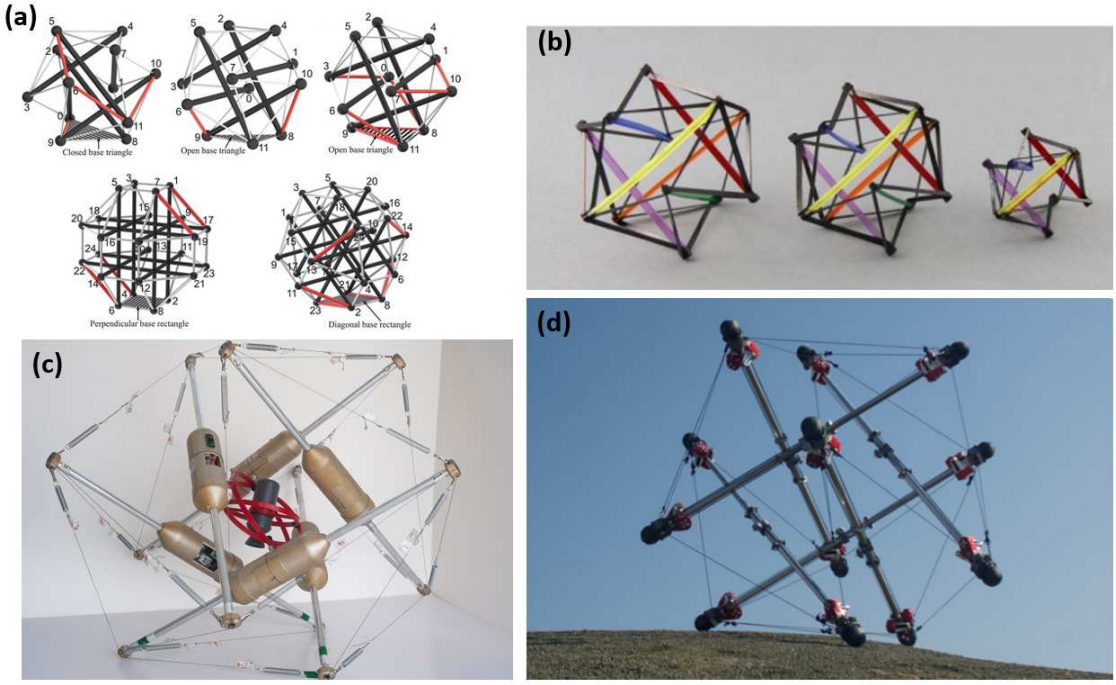

Figure 3.1: Various existing tensegrity robots and structures [15, 40]. (a) examples of spherical tensegrity structures ranging from six to twelve links []. (b) Light powered artificial muscle actuated tensegrity robot. Berkeley's Super Ball Bot, versions two (c) and three (d) [].

The term tensegrity was coined by American architect Buckminster Fuller in the 1960s and is a portmanteau for tensional-integrity. Tensegrity structures are combinations of rigid “compressive members” that are held together and in place by elastic “tensile members”. This combination of rigid links and elastic tensioners has been believed by many to be "Nature’s preferred design scheme" as it is found to have evolved independently in a multitude of different organic body systems [41]. For example, tensegrity systems can be found on a macro-scale in muscular-skeletal systems where rigid bones are held together under tension by muscles, tendons, and ligaments, or on a micro-scale in the cellular tensegrity model which suggests that rigid actin filament bundles are held together and under tension by elastic actomyosin [42].

There are many inherent advantages of tensegrity structures and mechanisms. For instance, when strictly straight rigid members are used, they experience exclusively axial loading. This means there is no bending moment present in any part of the structure and thus no shear stresses in the system, which makes it easy to optimize these rigid members’ materials and geometries for a specific loading application. There are currently many different designs of tensegrity structure being used in robotics, ranging from relatively simple 2-link systems to 12 and 24-link systems. Increasing the number of links increases the complexity of the robot as well as the resolution of a desirable path of locomotion. This project encompasses a rolling 6-link “spherical” icosahedron tensegrity robot. Research on a similar robot found that the load capacity to weight ratio is much higher for tensegrity robots compared to traditional robots or even vehicles [15]. Not only are tensegrity robots generally lightweight, but they are also deployable which is extremely advantageous for applications where weight and size restraints are of high importance, such as space exploration [33, 40]. Due to the low body density and lightweight, highly compliant nature of spherical tensegrity robots, they are ideal for absorbing and distributing impact energy (such as ground collision after a substantial fall) [43]. On contact, the impact energy on a given rigid link is transferred to motion and further distributed into a combination of the 6 elastic members attached to it, and then eventually surrounding links. The forces in each hyperelastic tensional member drive the robot to return to an equilibrium state, which is its original icosahedral shape.

Our free stroke TCAs were a prime candidate for actuating a tensegrity robot as they have many advantages over alternate forms of actuation. Because they are simple and made from common materials like nylon thread or fishing line, TCAs are relatively cheap to produce. They have a large work density similar to that of a jet engine at about 5.3 kW/kg and can produce a force some 100 times larger than a human muscle of the same length and weight [28]. They are actuated using a low voltage power source [20] and can simultaneously act as sensors to provide information about their displacement/deformation [44]. TCAs produce no noise or visible emissions and unlike traditional actuators, TCAs are made of non-compliant materials making them ideal for soft robotic applications. Free stroke TCAs specifically, are unique in that they do not need to be pre-strained to achieve a large actuation displacement of about 50% their natural length and can be embedded into soft bodies adding minimal strain to the systems. [20].

3.2 Design

A six-link spherical tensegrity robot is actually an icosahedron, where its 20 sides are categorized as 12 "open" triangles (two of the three edges have a TCA or spring along them) and 8 "closed" triangles (a TCA or spring on all three edges). Of the 8 closed triangles, four are designated counter-clockwise (CCW) and four are designated clockwise (CW), the implications of which are discussed in the results section below. The TR was designed on a small scale (10 cm diameter) to keep the overall weight down so that a single TCA could be used for actuation between two nodes. One high-priority design consideration was that the robot was built in a modular fashion to make repairing and replacing components time effective. The first prototype of the robot was built using silicone tubes to act as simulated TCAs so that various actuation policies could be verified on a simpler robot. Lightweight materials were selected for the TR to reduce the influence of mass on actuation.

The most technical parts of the TR were the 12 hubs that acted as mechanical connections for the tensional elements and held the electrical connectors for the TCAs. In the earliest ideation stage of designing the hubs, several designs were developed and assessed using a Pugh decision matrix

Determine ideal TR hub/TCA design		Hub as clamp design	Molex connector design	JST hook design original	JST hooks with sliding crimp
Electrical connetion speed and repeatablitly	25	-1	1	1	1
Mechanical connection speed and repeatablitly	25	-1	1	1	1
TCA termination angle	15	1	-1	1	1
TCA termination position	10	1	-1	1	1
Wiring management	10	0	1	0	0
TCA tension adjustment	15	1	-1	0	1
Total criterion		1	0	4	5
Total weight		-10	20	75	90

Figure 3.2: A Pugh decision matrix used to design the tensegrity robot hubs.

Figure 3.2. Six design criteria were established and weighted for importance then each design was scored according to how well it satisfied the design criteria. The criteria were as follows: the speed and repeatability of the electrical connections, the speed and repeatability of the mechanical connections, the TCA termination angle, the TCA termination location, wiring management, and having a TCA tension adjustment.

The rigid links or "rods" were made from 3 mm carbon fiber round rod stock. An arbitrary rod length of 100 mm was selected and a stretched length of 61 mm for the synthetic TCA's was calculated using the following equation where l_{cable} is the length of the cable and l_{rod} is the length of the rod:

$$l_{cable}/l_{rod} = \sqrt{(4x^2 - 2x + 1)/2} \geq 0.61 \tag{3.1}$$

The simulated TCAs were made using (.020" ID x .036" OD) silicone tubes. A spring constant for the elastic tube was experimentally determined to be .0125 N/mm. In order to provide a resting state tension of 0.2 N, the following equation was used to determine the unstretched tube length:

$$F/k = \delta x = 0.2N/.0125 = 16mm \tag{3.2}$$

Where F is the tensile force of the tube, k is the spring constant, and δx is the change in length that produces said force. The tubes were cut to an initial length of 45 mm and each tube was fitted with a metal hook so they could be easily replaced or moved on the connectors. The rod end connectors or "hubs" were designed in Solidworks and twelve were printed using a Prusa i3 MK3 Fused Filament Fabrication (FFF) printer and polylactic acid (PLA) material. The hubs were designed as mechanical connectors to hold the hooks of simulated TCAs as well as the electrical connector pins of the actual TCAs. Once all of the components were fabricated, the tensegrity icosahedron was assembled.

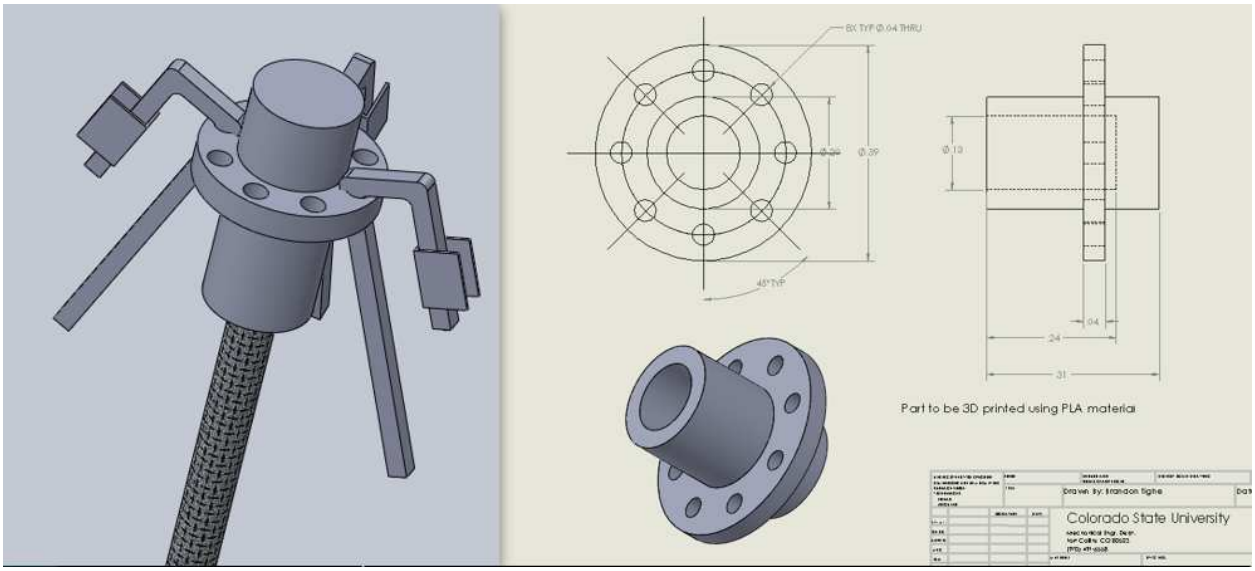

Figure 3.3: Model and design of the tensegrity robot mechanical and electrical connectors, or "hubs". The CAD model on the left shows a hub fixed onto a carbon fiber rod along with 3 JST pins connected.

Several meters of Type 1-180 TCAs (α_m=15.57%) were fabricated using the CNC-controlled machine discussed in Chapter 2. We selected Type 1-180 TCAs because they were able to produce a larger actuation force than Type 2 TCAs while still providing an adequate dynamic response. After being fabricated, annealed, and prepared, the TCAs were cut to an ideal length of 60 mm. Next, the TCAs were terminated at either end by inserting 0.6 mm Japan Solderless Terminal (JST) pins into three end coils of a TCA and glued in place. The JST pins act to mechanically connect the TCAs to the hubs and as electrical connections to pass current through them, as seen in Figure 3.3.

This resulted in a 55 mm effective actuator length. Two TCAs were strategically placed on the tensegrity structure (one along an edge of the open base triangle, and another along the edge of an adjacent closed base triangle) to produce three specific types of steps.

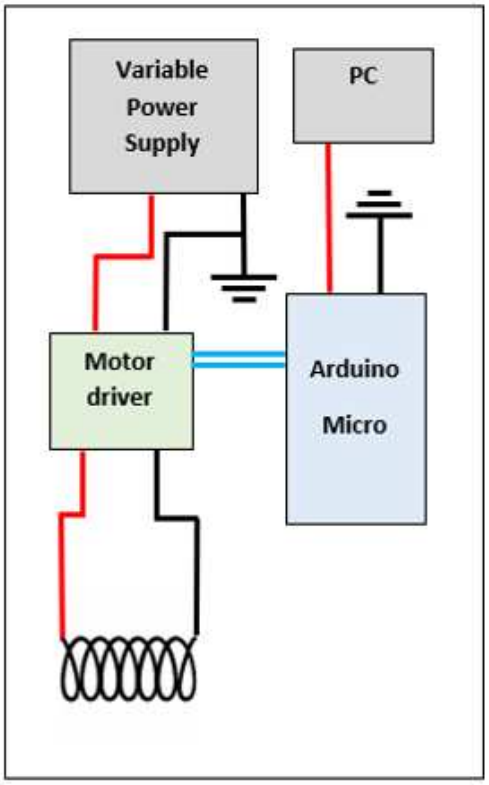

Figure 3.4: The simple open loop control system used to actuate the tensegrity robots TCAs. An operator manually selects which TCA to actuate using a keyboard, and an Arduino sub-routine passes current through the TCA via the motor drivers for a pre-determined amount of time.

A simple open-loop controller was built using an Arduino Micro microcontroller. Current was supplied to the TCAs using Pololu DRV8833 dual motor drivers using a DC regulated variable power supply as shown in the schematic Figure 3.4. We wrote the open-loop control program to leverage Arduino's Serial Monitor tool so that we could independently control up to 24 TCAs.

There were some problems with the first iteration of the tensegrity robot that required some minor component redesigns to fix. The first problem was that a particular type of step required a simulated TCA adjacent to an activated one to stretch 1.4 times its natural length which demanded more force than our actuator could provide. This was remedied by replacing the original tube

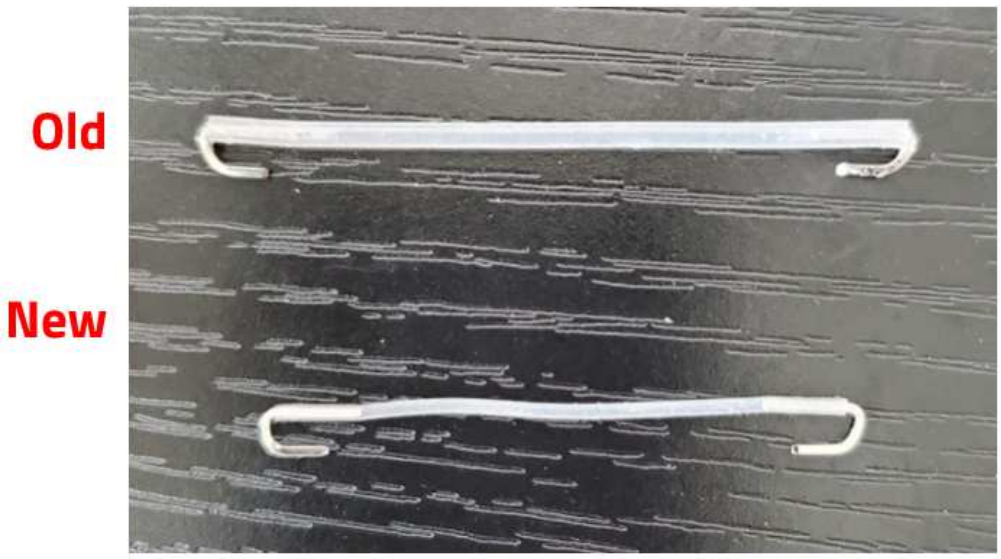

Figure 3.5: The new simulated TCA resulted in a 50% component weight reduction and produced a 70% lower reaction force against the TCA.

with one that had a 73% smaller cross-sectional area and thus required less force to displace. The new simulated TCAs resulted in a 50% component weight reduction and required a 70% lighter actuation force to overcome.

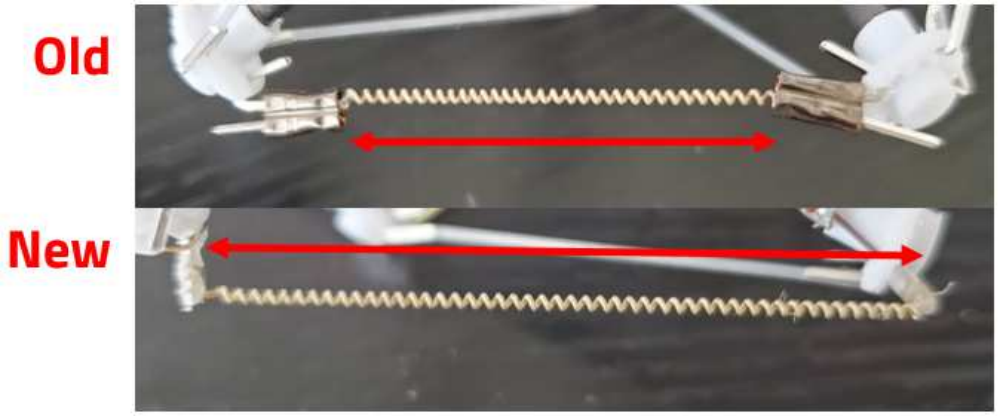

Figure 3.6: The new method of connecting the TCAs to the robot resulted in an 80% component weight reduction and increased the effective length and potential displacement of the TCA by 49%.

The second problem was that the electrical and mechanical connector design limited the effective actuator length, thus lowering the maximum stroke length that we could produce so we were not able to attain the 36% contraction that we needed to initiate a roll. Also, the connectors

were heavy enough to influence the center of mass of the robot, rendering our actuation policies inaccurate. A redesign of the TCA connector addressed both of these issues and resulted in a 49% increase in effective length as well as an 80% component weight reduction.

3.3 Actuation Policies

Because of the complex nature of a tensegrity robot (and soft robotics in general), it has taken much effort to identify accurate and effective actuation policies. Early tensegrity robot work used experimentation to derive actuation policies [45, 46], but recently, more advanced techniques have been utilized. NASA produced an open-source tensegrity structure modeling software known as Nasa Tensegrity Robot Toolbox, which researchers used in correlation with Monte Carlo and greedy search machine learning algorithms to develop a complete theoretical set of actuation policies. The greedy search algorithm is based on a heuristic function which is defined as the distance between the gravitational center of mass (GCoM) and the edge of the base triangle defined as the axis of rotation. When the heuristic distance approaches zero, a roll is assumed. Actuated edges were simplified into binary states of fully extended or contracted, and usable actuation polices were developed Figure 3.7.

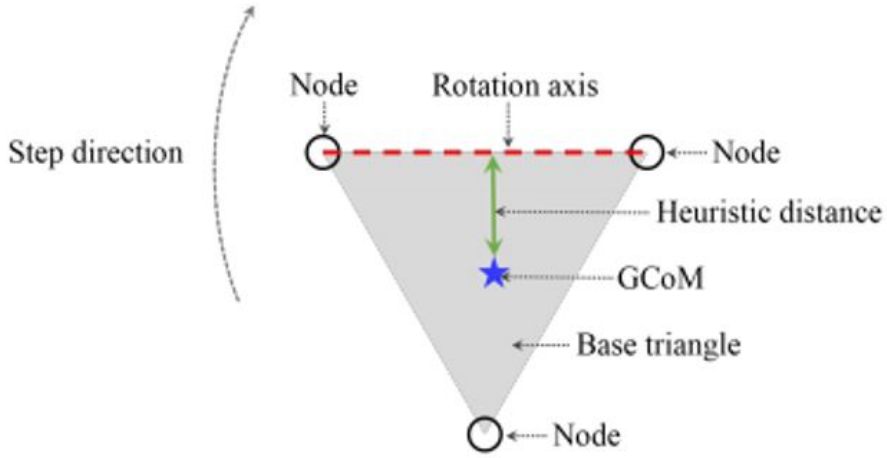

Figure 3.7: Model used for actuation policy development using a greedy search algorithm. The gravitational center of mass (GCoM) moves away from the center of the base triangle as the robot body deforms and a roll is initiated when the GCoM passes over an edge. This figure is sourced from [40].

Numerical methods such as dynamic relaxation have also been used as a basis for determining theoretical actuation policies [15,40]. Researchers developed a mass-spring network made with 12 point masses representing each node or hub, 24 hyperelastic springs representing the elastic tensile members, and 6 stiff elastic springs representing the rigid compressive members. The position of one point mass is represented r_i and its mass by m_i. The force balance for the system of mass points is written:

$$m_i\ddot{r}_i + D_i r_i + \Sigma_j K_{ij}((|r_i - r_j|)/l_{ij}^0 - 1)\eta_{ij} = f_i \tag{3.3}$$

where D_i is the damping coefficient, $l_i j^0$ is the natural length of the spring, $f_i$is the external force,

$$n_{ij} = (r_i - r_j)/|r_i - r_j| \tag{3.4}$$

note: $K_{ij} = k_{spring}A_{TCA}$ if the point j is connected with i by TCA, and $K_{ij} = k_{stiff}A_{rod}$ if the point j is connected with i by a rod or finally K_{ij}=0 if the point j is not connected with point i.

where k_{spring} and k_{stiff} are the elastic moduli of the TCA and rod, respectively, and A_{TCA} and A_{rod} are the cross-sectional areas. With a given l_{ij}^0, the system of equations can be solved. For simplicity, set $m_i = 1$, and D_i is chosen to optimize quick relaxation of the TR. Assume gravity is negligible by setting f_i=0. When this system reaches an equilibrium state, (i.e. the actuated TCA is at critical contraction and the tensegrity robot's GCoM is located directly above a base triangle's edge), further actuation results in rolling over the base triangle's edge. That critical stretch of the TCA is the basis for our actuator stroke length and these theoretical predictions agree with the machine learning actuation policies as discussed above.

3.4 Results and Discussion

With two TCA's attached to the robot, we were able to achieve a step type with each of three possible start and end conditions, as shown in Figure 3.8. This is significant because it validates each of the actuation policies is accurate for the general case, load-free locomotion on flat, level

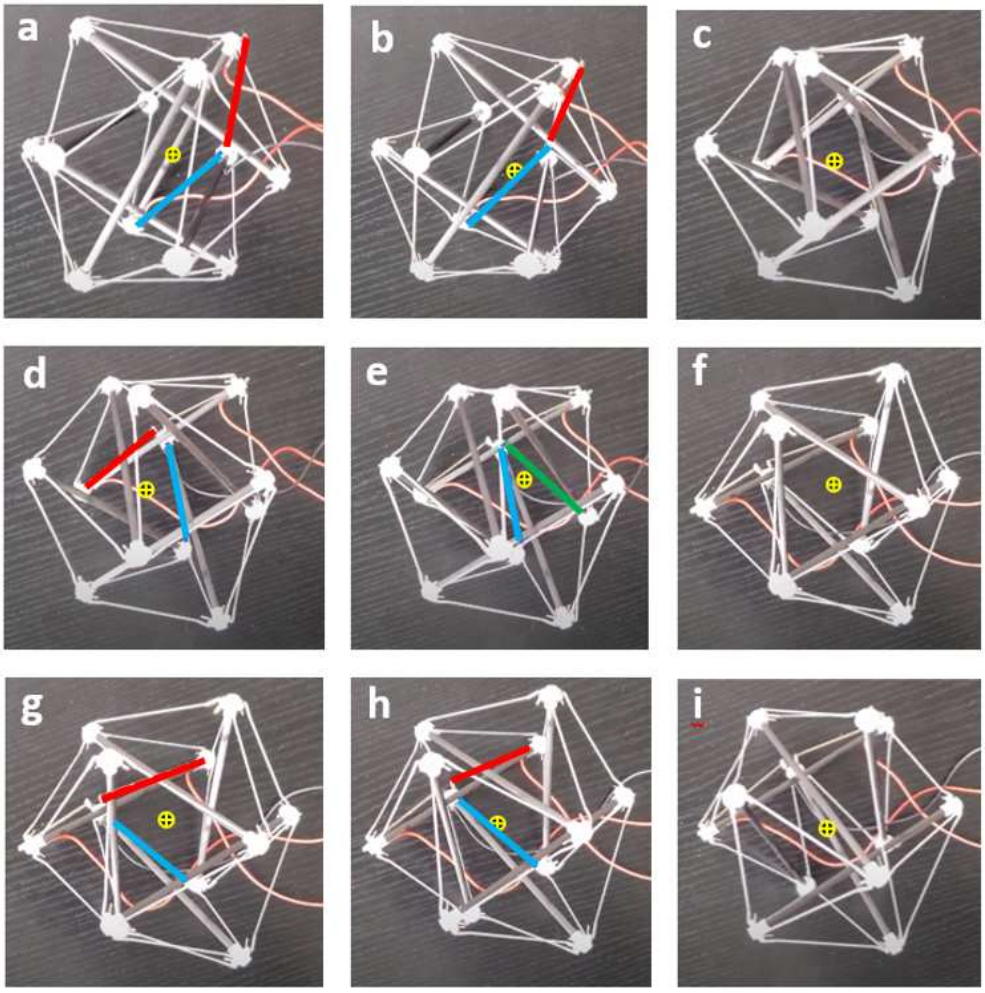

Figure 3.8: Detailing the initiation of a roll with the 3 possible start and end conditions. Red lines represent an actuated TCA, blue and green lines represent the rolling axis of the TR, and the yellow dot represents the GCoM. (a-c) An open-to-closed base triangle step type is realized, note that rolling is initiated in (b) when the GCoM reaches the axis of rotation. (d-f) A closed-to-closed base triangle step type, where angular momentum produces two steps with a single actuation event. (g-i) A closed-to-open base triangle step type.

ground. The three types of steps achieved are an open-to-closed base triangle (Figure 3.8 a-c), a closed-to-open base triangle (Figure 3.8 g-i), and a closed-to-closed base triangle configuration, which is notable because it leverages rotational momentum to achieve two steps from a single actuation (Figure 3.8 d-f).

During an open-to-closed step, the robot can roll over either of the two "closed" faces of the base triangle by actuating a single TCA. The blue line in Figure 3.8a would be the axis of rotation, the red line is the actuated TCA, and the yellow dot is the gravitational center of mass (GCoM). At

the start of actuation, the robot is essentially symmetrical so the GCoM is located at the center of the base triangle. In Figure 3.8b the robot body is deformed to the point where the GCoM is about to cross the edge of the base triangle. When this happens, a roll is initiated. Figure 3.8c shows the robot settled at the end orientation of the step, a closed base triangle.

A closed-to-closed base triangle step can be produced by initiating a roll from the closed base triangle orientation towards an open base triangle. By using higher voltages, the TCA contracts faster and the robot utilizes rotational inertia to continue rolling over the open base triangle onto a second closed triangle. Figure 3.8d shows the robot in a closed base triangle orientation with the GCoM centered. Unlike rolling from an open base triangle, the TCA used to produce a step is one of the edges of the base triangle. The green line in Figure 3.8e highlights the axis of passive rotation. This image shows the middle of the roll, just before rotational inertia passively rolls the robot into its end orientation Figure 3.8f.

A closed-to-open triangle is the simplest roll and it is realized the same way as the closed-to-closed roll, but with lower voltages so that the robot stops on the open base triangle. Figure 3.8g shows the starting orientation, Figure 3.8h is the moment before the robots GCoM crosses the blue axis of rotation. Figure 3.8i is the end condition with the GCoM centered on the open base triangle.

Starting from an open base triangle, the robot can move in one of two different directions (over either edge that has a tensional element along it), whereas with a closed base triangle, the robot can roll over any of the three base edges(each active edge is a respective axis of rotation). Employing various combinations of these three-step types can result in locomotion along simple and complex paths. Figure 3.9 illustrates how a combination of straight paths, and left and right turns can result in more complex maneuvers such as obstacle avoidance.

Using TCAs to actuate the TR proved to be advantageous for multiple reasons. This method of actuation was able to achieve three consecutive steps some 300% faster than another group's light-activated artificial muscle TR, plus this technology is a candidate for a fully self-contained system [15]. TCA actuation is silent which could be useful where device detection or audible noise

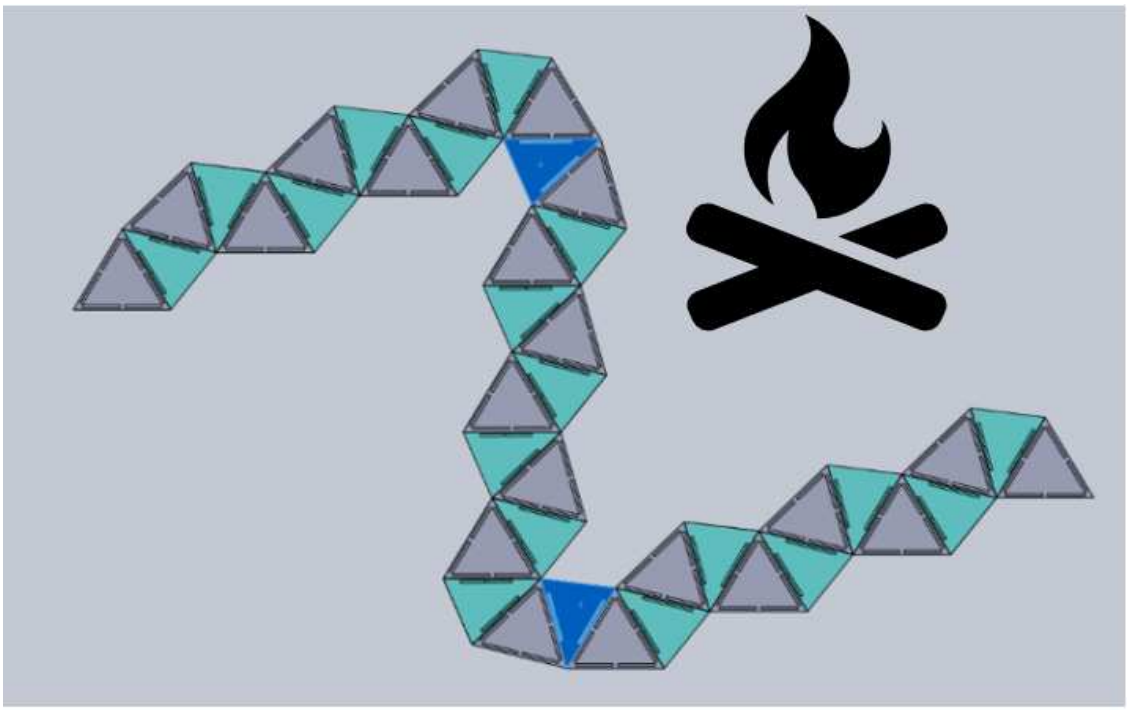

Figure 3.9: An example of how a path can be generated by using specific consecutive steps to travel in a straight line or avoid an object.

is of concern. Another advantage of this design is how lightweight it is, this robot has a density of just 1.4 kg/m^3, largely due to its open interior and lightweight materials.

Some challenges came with the TCA TR design, for instance, single a single TCA will have force and displacement limitations that cannot be overcome with design alone. In order to make this model into a large-scale TR (>1m) we would have to use multiple TCAs in parallel to produce the forces required for locomotion. We were also limited to a maximum stroke length of 50%, which limits the usable actuation policies that are available to us (some TR designs use a stroke length of 90% or more to traverse certain environments). This specific configuration of TCA did not allow for high enough strain to be able to replace all 24 simulated TCA's with working actuators.

A continuation of this work may include re-designing the TCAs with a larger spring index so that they will be able to elastically stretch enough so that we can operate the TR with all 24 actuators in place. Redesigning the mechanical connection hubs at the end of each rod would allow for optimal actuator placement as well as minimize TCA-surface interactions. Eventually,

this project may include untethering the robot by bringing the electrical components on board, or adding force and orientation sensors that can be used in conjunction with the TCA's state sensor functionality to achieve closed-loop control for locomotion and state identification.

3.5 Conclusion

In conclusion, the twisted and coiled actuator tensegrity robot model proved viable and advantageous. Coupling artificial muscle linear actuators with the biologically inspired robot design succeeded in addressing some of the issues with the current six-link icosahedral TRs, including their limited downsize scalability, noisy and slow actuation, and ability to be fully self-contained systems. We were able to successfully and consecutively realize three different step types with our TCA-driven tensegrity robot, being a closed-to-closed base triangle step, a closed-to-open base triangle step, and an open-to-open base triangle step.

Further work on this project may involve leveraging the TCAs displacement sensing function to implement closed-loop control. It may also involve bringing the controls and power on board to untether the robot. There is currently a lot of interest in tensegrity robots for space exploration, so this project could likely start addressing some of the challenges therein such as accurately controlling the TCAs over a wide range of external temperatures.

Chapter 4

Soft Robot Application: Multimodal Shape Morphing Robot

4.1 Introduction

Robots typically employ a single mode of locomotion, such as the countless rolling, crawling, or flying robots we see around us. Some multimodal robots are emerging that take advantage of two modes of locomotion such as Stanford's SCAMP robot which uses a quadcopter to fly and can drag itself along a vertical surface to climb [47], a millimeter-scale soft-bodied robot that uses magnetic fields to change its shape for crawling and rolling [48], or DALER which is a propeller-driven flying robot that uses its wingtips to crawl [49], but none seem to utilize a biologically inspired approach. The notion of a robot with only one or two modes of locomotion limits the obstacles and environments in which they can explore and contrasts the way many animals traverse various environments by walking, running, crawling, jumping, and swimming. The emerging field of biologically inspired robotics has brought new knowledge to biologists and roboticists alike. For this project, we attempted to mimic animalistic quadrupedal locomotion.

It was imperative for us to do background research on typical modes of quadrupedal locomotion. A significant amount of research has been done studying various animals and how and why they use their different types of locomotion [11, 50, 51]. Intending to realize three different modes of locomotion, we started with an overview of different types of locomotion (crawling, flying, swimming, walking, climbing, etc.) and narrowed the most achievable modes to be walking, crawling, and climbing. We next broke down each mode of locomotion into different types and studied details such as what the gait patterns look like, if they are static or dynamic gaits, how fast a cyclic period was, and how much displacement and force is required to realize a step. After gaining a general understanding of these various modes of locomotion, the next step was to design

and fabricate a robot that could alter its mechanical shape (i.e. body posture) to realize various modes of locomotion.

To organize the project, we divided it into several tasks, each with its own specific aims. First, we wanted to make a lightweight, artificial muscle-driven 3D bending module to be used as the robot's legs. The bending modules needed to be stiff enough to hold the weight of the robot and needed to be able to produce a loop foot trajectory with enough foot displacement to lift off the ground. Further, we needed the modules to be able to execute a full step cycle quickly (< 2 s) in order to realize dynamic gaits. Our second specific aim was to design shape morphing modules that could execute and maintain a variety of shape changes. The modules needed to be lightweight and be able to reliably sustain rigid shapes for long periods of time, using little to no energy. Next, we wanted to design a lightweight, rigid body that could combine the 3D bending legs and shape morphing modules, as well as organize the wires and tether. We needed to create an electrical control system that was capable of providing independent and simultaneous power to 12 TCAs and three shape morphing modules. The control system also needed to be able to quickly execute a large number of routines. Finally, after successfully building the robot, we wanted to design and make an obstacle course to demonstrate various modes of locomotion and conduct experiments to characterize different aspects of the robot's components.

4.2 Artificial Muscle Driven Robotic Legs

4.2.1 Working Principles of Leg Module

Similar to the 2D bending soft actuation method mentioned in chapter one [11], the general working principle of our bending module is to cause linear displacement on one side of a mechanism and effectively none on the other. We accomplish this by attaching a linear actuator longitudinally along an axially stiff, yet bendable strain limiting layer. Two-dimensional bending occurs when the linear actuator creates a displacement and the strain limiter does not. To achieve the 3D bending necessary for creating a loop trajectory, we evenly spaced and placed three TCAs around a strain limiting rod. The TCAs are held in place at a set distance from the neutral axis by triangular

plates that we call vertebrae. Each TCA is wired for an independent voltage supply and all are terminated to a common ground. When a current is passed through a given TCA it heats up and contracts, bending the leg in the direction of the actuator.

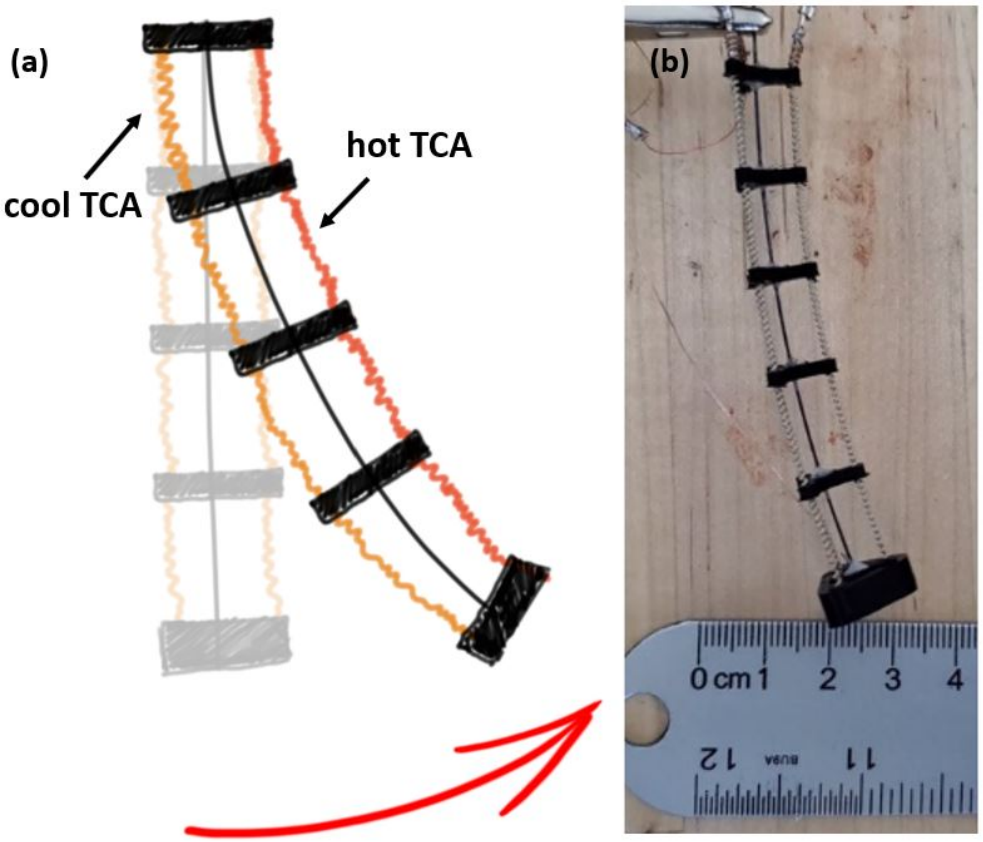

Figure 4.1: (a) Illustration of the working principles of the 3D bending module. As the rightmost TCA is actuated, its compressive displacement is converted into bending. (b) A fabricated 3D bending leg shown producing 20mm of foot displacement.

4.2.2 Design and Fabrication

Before making the legs, we defined the design considerations, which were primarily based on functionality. We wanted to use TCAs to illustrate some of their advantages such as being lightweight and using low energy. We wanted each leg to be lightweight, be able to hold about 15 g (50% of the robot's weight) when the robot was in a walking orientation. We also needed to be able to produce at least 2.5 cm of foot displacement to create a loop foot trajectory while in the

walking orientation. The legs needed to be designed in such a way that the TCAs were exposed to open air (i.e. not embedded in a soft body) so that we could use forced convection to actively cool and reverse the contraction of the TCA quickly so that we could increase our achievable actuation frequency. We also wanted the legs to be modular so that we could repair or replace components quickly and easily.

We utilized additive manufacturing for all of the custom parts as it is fast, affordable, and convenient for prototyping. The majority of our unique parts were made using a Prusa i3 mk3 melt-extrusion printer and polylactic acid (PLA) filament. We chose PLA because it is lightweight, relatively hard, is easy to print with, and has minimal warping. The only 3D printed parts that we could not make with PLA were the vertebrae (Figure 4.2) since they come in direct contact with the TCAs. The glass transition temperature of PLA is 60°C and the highest actuation temperature of a TCA is about 160°C, which would certainly result in part failure. To avoid this we used a thermoset material in lieu of a thermoplastic and printed the parts on a photopolymer printer (specifically, a Prusa SL1 speed). We used Siraya Tech high-temperature resin, which withstands temperatures up to 220°C). The strain limiting component of the bending modules was made of 0.5 mm diameter carbon fiber rod and each TCA was terminated using 32 gauge copper wire and 0.6 mm JST pins.

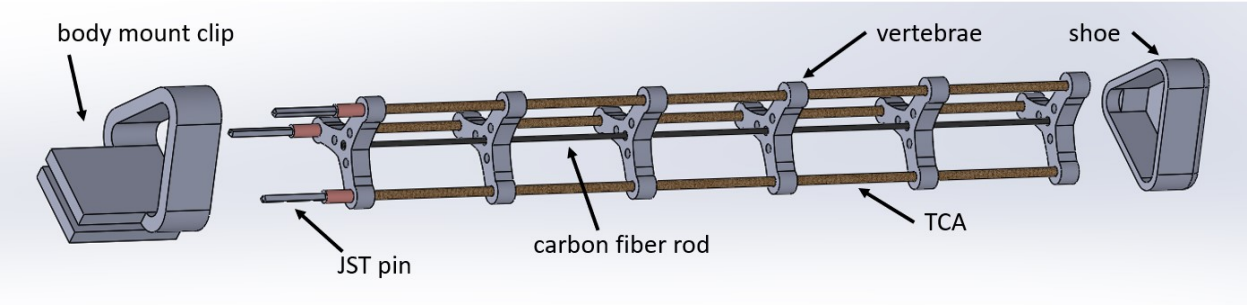

Figure 4.2: CAD model of the leg assembly.

The legs were designed to be 90 mm in length which allowed for adequate foot displacement while still being stiff enough to hold the weight of the robot when it is in a walking orientation. The distance between the carbon fiber spine and the TCA acts as a moment arm and directly affects

the amount of bending displacement and force that is produced when a TCA is actuated. Each leg has seven evenly spaced vertebrae along the spine that hold the three TCAs at a set distance of 5.5 mm from the neutral axis. The end of each leg is capped off with a 5 mm deep shoe which houses the three TCAs ground terminals. The inner edge of the shoe and the first vertebrae has a strip of silicone attached to it which increases the friction coefficient against the ground while the robot is crawling.

Each leg consists of a 90 mm carbon fiber rod, seven vertebrae, a "shoe", a clip that is used to mount it to the body, and three TCAs. A jig is used to evenly space and orient the vertebrae along the spine before they are glued into place. Although the legs are 90 mm long, 105 mm lengths of TCA are used because they shrink approximately 15% after they are trained. To make the positive terminal, a 0.6 mm JST pin is inserted into three coils of each TCA and is then tied in place using copper wire. The TCAs are then inserted through the receiving holes on the vertebrae and terminated on the negative end by placing a 7 mm long, 16 gauge copper core into the bottom 4 coils and securing it with 32 gauge wire. The negative terminals of the TCAs are all connected together with a length of 32 gauge wire that runs along the spine back to the positive end and has a JST pin soldered to it. After wiring in the TCAs, the shoe is press-fit onto the bottom vertebrae and the body mounting clip is press-fit onto the top.

4.2.3 Results

With the appropriate actuation sequence, the 3D bending module can execute the loop foot trajectory that is necessary for walking or crawling. To explain the actuation policy, I will use the naming convention TCA 1, TCA 2, TCA 3- with TCA 1 being the frontmost TCA, and TCAs 2 and 3 towards the rear of the robot, as seen in Figure 4.2.

The open-loop policy for the walking, crawling, and shimmy gaits are slightly different but all incorporate the loop foot trajectory. The policy for walking begins by actuating TCA 2 for 600 ms, which lifts the foot, then actuating TCA 2 and TCA 1 together for 600 ms, which brings the foot up and forward. Next, TCA 1 is actuated for 600 ms bringing the foot down and forward, and then

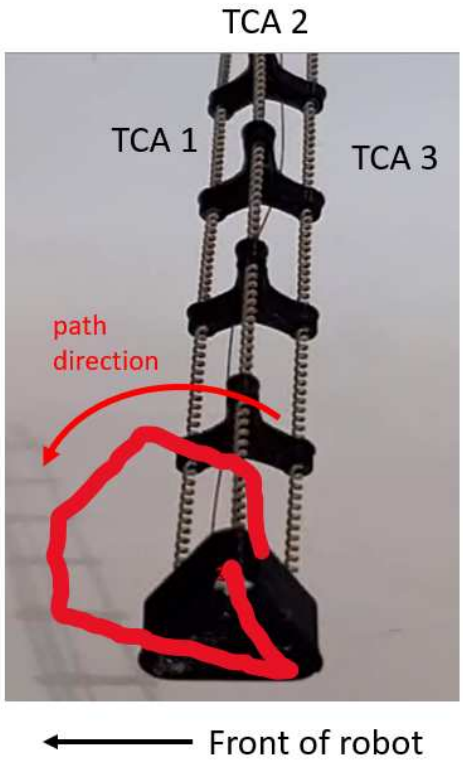

Figure 4.3: Foot trajectory obtained using video analysis. The TCA naming convention starts with number 1 towards the front of the robot and 2 and 3 are towards the rear. Note that the actuation policy used here consisted of 5 segments of actuation, opposed to the more symmetrical 6 segmented policies that were used for crawling and walking.

TCA 1 and TCA 3 are actuated for 600 ms which brings the foot straight down. Next, TCA 3 is actuated for 600 ms which brings the foot down and back. Finally, TCA 3 and TCA 2 are actuated together for 600 ms which moves the foot back and up, then the cycle begins again by actuating TCA 2 alone.

The actuation policy for crawling is similar to the policy for walking, although instead of being split into 6 temporally equidistant segments, there is an asymmetrical actuation time for the TCAs. The crawling policy emphasizes the initial lifting of the foot by beginning with actuating TCA 2 for 1000 ms, then continues similarly to the walking gait (600 ms segments), aside from the last segment which is 300 ms. This was necessary to lift the feet high enough that they would come off the ground completely.

4.3 Shape Morphing Module

4.3.1 Working Principles of a Shape Morphing Module

The shape morphing modules (SMM) combine an artificial muscle-driven 2D bending module with the ability to maintain a shape without additional energy. To accomplish this we use a shape memory polymer spine as the strain limiting layer and have a TCA aligned longitudinally along it that is attached at both ends. We first heat the shape memory polymer spine so that it becomes compliant and can easily bend (Figure 4.4b). When the SMP spine reaches 120°C, actuate the TCA to the desired displacement (Figure 4.4c) and hold it there by maintaining its temperature while the spine cools and regains its rigidity (Figure 4.4d). To return to its original shape, we simply heat the spine again and the actuation force of the shape memory polymer returns it to its straightened shape.

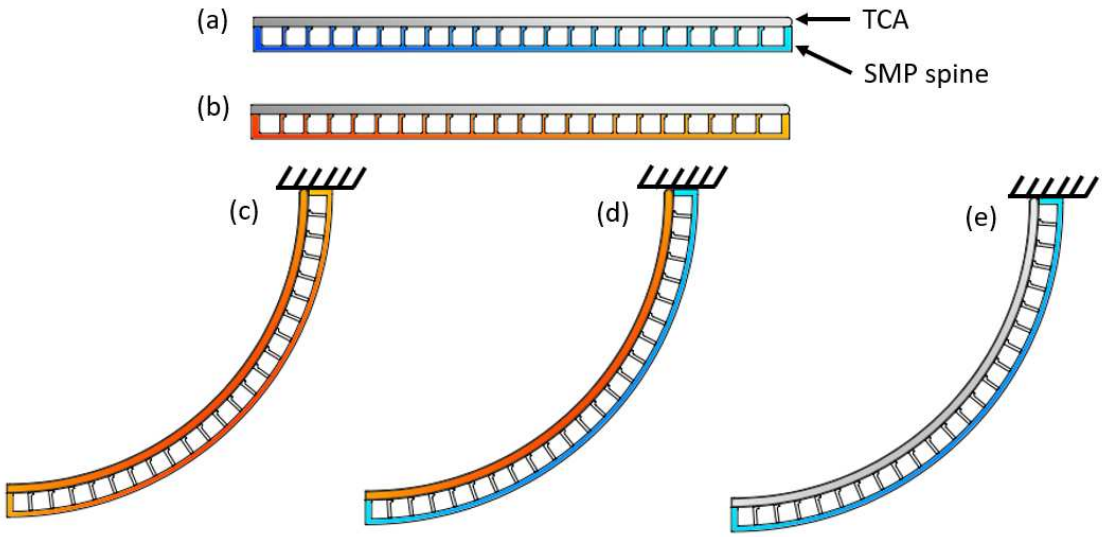

Figure 4.4: The working principles of a shape morphing module. (a) The straight module in its cool, rigid state. (b) Using resistive wire to heat and soften the shape memory polymer spine. (c) Once the spine reaches 120°C, actuate the TCA to promote bending. (d) Maintain the temperature of the TCA to hold the bent position while the spine cools. (e) A bent module in its cool, rigid state.

4.3.2 Design and Fabrication

We needed the SMM to be able to change from a relatively flat shape (at approximately 10°from straight) to a curved one (about 200°bend) and to be able to return to its original shape. We wanted the SMM to be able to maintain various shapes without needing to be constantly powered. Another design consideration was that we had to be able to accurately and independently control the temperature of the TCA and the polymer spine. The modules needed to be as lightweight as possible to minimize the robot's overall weight. It was crucial for the SMM to produce enough bending force to stand the robot up and clamp the legs onto a beam. Like the legs, we wanted the SMM to be modular so that we could conveniently replace and repair damaged components.

TCAs were a perfect candidate for our choice of linear actuator as they are lightweight, produce adequate and repeatable displacements, and can be cycled thousands of times. We wanted to terminate the TCAs with JST pins to provide reliable quick-change connections. We chose to use a shape memory polymer as opposed to a thermoplastic for the SMM spine so that the SMM could recover to its original shape without needing an antagonistically oriented TCA. We embedded the TCAs into thin silicone tubes so that we could glue them to the spine and still allow the TCA to slide freely between attachment points. We chose to use Ecoflex 30 silicone because of its high temperature rating and hyperelasticity. We opted to use resistive wire to heat the spine, specifically 26 gauge Nitinol (NiTi) wire, as it provides consistent, uniform heat using relatively low currents.

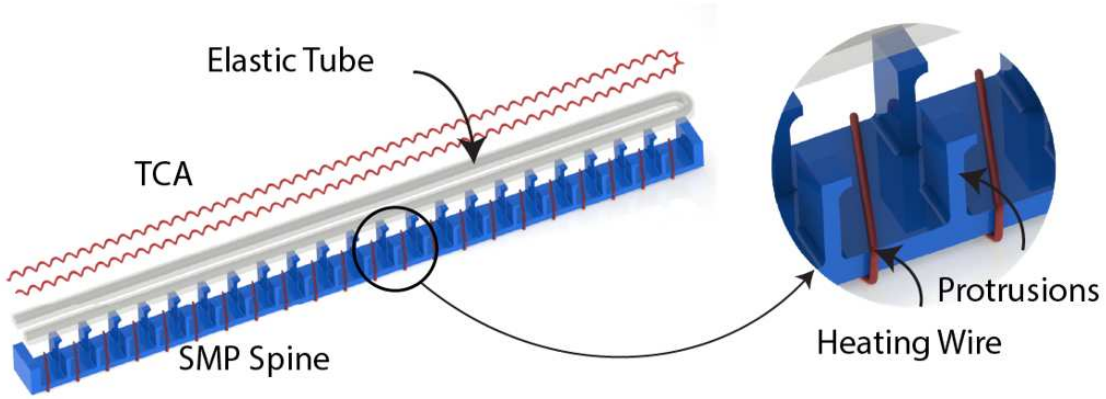

Figure 4.5: Components of a shape morphing module.

The length of the SMM is directly proportional to its bend radius, and the primary driver in deciding what length to make the modules was the maximum bending angle it could produce. We determined that a 113 mm module could produce over 200°of bending. The thickness of the spine was crucial in allowing it to bend without breaking, a thin spine could bend with a very small radius but too thin of a spine would not produce enough recovery force to straighten the spine. We experimentally determined that a 1.2 mm thick spine was ideal for being able to withstand the maximum bending our project required and with a width of 7mm, the spine could provide enough recovery force to return a bent module to its original shape. Similar to the 3D bending legs, the distance between the TCA and the spine affects the bending angle and force required to achieve it. A shorter distance can produce large bending with little TCA displacement, whereas a longer distance provides less bending displacement but requires less actuation force from the TCA. We designed the SMP spine to have transverse protrusions along its length to hold the TCA 5mm away from the spine, which allowed for adequate displacement and required low enough of an actuation force that the module could be cycled hundreds of times without damaging the TCA. Further, we designed the protrusions to have minimal volume, with an open body design, which functioned to minimize the amount of heat that was convected from an actuated TCA to the spine, thus lowering the time it takes to cool off and become rigid after a heating cycle. The silicone tube that encased the TCA was installed with 28% pre-stretch which contributed to the bending force produced by the TCA and prevented the tube from experiencing excessive compressive forces (that would oppose bending).

The first step in building the SMM was to CAD design and 3D print a blank of the spine to be used for making a silicone mold. We used a Prusa SL1 Speed photopolymer printer as it has a very high resolution that results in smooth prints. After being post-processed and cleaned the spine blank is used to cast a mold out of Smooth-On Mold Star silicone. Once the silicone mold cures, we remove the blank, we make the shape memory polymer by mixing EPON 828 epoxy with a 6% weight ratio of the hardener diethylaminopropylamine. We then pour it into the mold and cure it at 75°C for 12 hours. Because of the small features of the spine, it is necessary to use a vacuum oven

to cure the SMP spines, as the negative pressure helps to remove bubbles from the mold. After the SMP spine is cured and carefully removed from the silicone mold, we use 32 gauge copper wire to secure the NiTi wire to one side of the spine, which holds it in place and acts as a low resistance terminal. Next, we wrap the resistive wire around the spine in a helical fashion, being careful to space the coils evenly and keep the same number of total coils on each module. Having the same length resistive wire on each module was crucial for this project as the robot used 3 SMM wired in parallel and any length discrepancies would result in uneven heating of the modules. After fully wrapping the spine with NiTi wire, the end is terminated using copper wire to anchor it to the spine. Next, we prepare a 255 mm TCA by terminating one end with a JST pin and the other with 10 cm of 32 gauge copper wire. We use Ecoflex 30, a 3D printed mold, and carbon fiber rod cores to make thin-walled silicone tubes (1mm ID x 2mm OD). The terminated TCA is then embedded into a 160 mm length of the silicone tube and is fixed at either end using Sil-Poxy silicone glue. Next, we stretch the tube and TCA and clip it to a 3Dprinted jig that holds it in position so that we can glue the tube to the protrusions of the SMP spine. Finally, after the silicon glue cures, the module is removed from the jig and ready to be connected to power for training and use.

4.3.3 Results

We experimentally determined that the ideal temperature for the SMM spine to be for bending is 115°C. If the spine is not hot enough, it will be too stiff and will result in a broken TCA, conversely, if the temperature is too high the shape memory polymer becomes brittle and breaks. The simplest way to bring the spine to the ideal temperature is to apply current through the resistive wire for a set amount of time, but the problem with that method is that factors such as ambient temperature and air velocity (i.e. wind) can be difficult to control and can contribute enough to prevent the spine from arriving at a usable temperature. To remedy this we used a Flir thermal camera to closely monitor the spines temperature.

Heating the spine and momentarily actuating a TCA to bend the SMM is relatively simple, but not entirely useful. What's more useful is to be able to heat and bend the spine, then hold

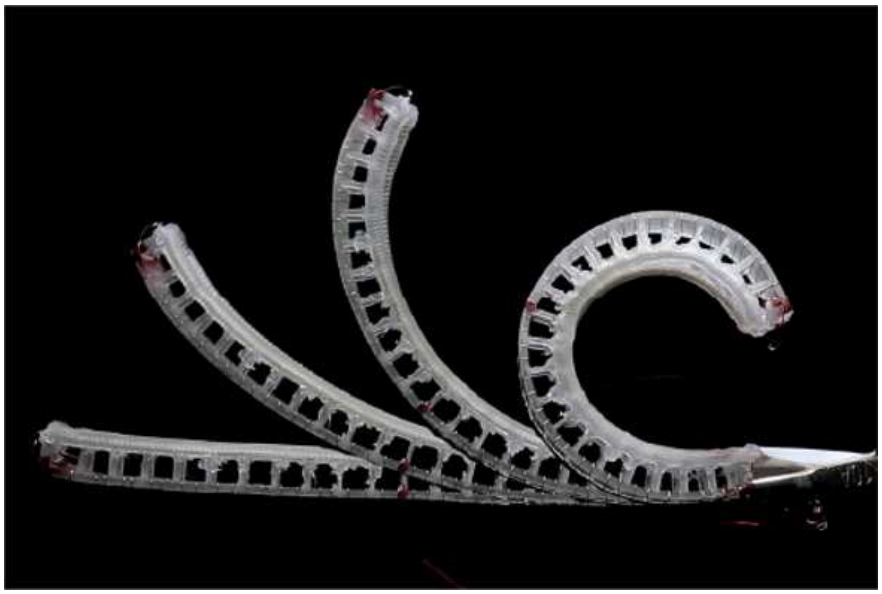

Figure 4.6: Snapshots of a shape morphing module taken from a characterization video.

that shape while the spine cools and becomes rigid again. The displacement of a TCA (and in this case, the SMMs bending angle) is directly proportionate to its temperature, so maintaining an exact TCA temperature is the key to holding a SMMs shape. Because the SMP is exposed to air, we could directly measure its temperature and experimentally find a coefficient to maintain its functional temperature in a set ambient condition. Since the TCA is embedded in a silicone tube, its actual temperature is first conducted through the silicone and we measure the temperature of the tube's surface as heat convects from it. This makes accurately maintaining the temperature of the TCA more difficult, but we developed a couple of different methods of doing so. The simplest method of doing so leverages the equilibrium point between the heat generated and heat lost through conduction and convection. A TCAs temperature is proportional to the current passing through it, and the rate at which heat is transferred from a system is proportional to the difference in temperature from both sides of the system ($\triangle_{hot} - \triangle_{cold}$), so there must exist corresponding voltages for desired temperatures. We experimentally quantified this for a non-loaded SMM by heating a spine to 115°C and adding various low voltages until the spine reached a steady-state as seen in Table 4.1.

Table 4.1: Experimental results showing various shape morphing module bending angles as a result of the TCA reaching thermal equilibrium under different voltages. Note this experiment was done on a non-loaded SMM.

Trial	Voltage [V]	Bending Angle [°]	Time [s]
1	0	70	100
2	0.22	90	100
3	0.45	108	100
4	0.67	135	100
5	0.89	163	100
6	1.11	185	100
7	1.34	235	100

With a quantified relationship between voltage and bending angle, we could theoretically heat a SMM, hold a bending angle, and then cool the SMM to hold that angle, but the process takes long enough that it is impractical for our application. To speed up the process, we initially heat the TCA at a higher actuation voltage of 13 V for enough time (such as in Figure 4.7) to reach the desired bending angle and then lower it periodically to maintain that angle. Further, we experimentally determined that the ideal rate to decrease voltage fit along a curve of exponential decay, and we used that knowledge to write an actuation policy that started with full voltage and incrementally lowered it to the shape maintaining voltage. Using this method of bringing a TCA to the desired temperature only took a couple of seconds, which is much faster than the previous method (100 s) and allowed us to fully morph the shape of the modules in a fraction of the time.

4.4 Shape Morphing Quadrupedal Robot

4.4.1 Investigation of Quadruped gaits

For decades, biologists and engineers alike have studied various animals and how and why they employ different gaits and modes of locomotion [11, 50, 51]. Intending to realize three unique modes of locomotion, we started with a comprehensive overview of different types of animalistic locomotion (crawling, flying, swimming, walking, climbing, jumping, inching, etc.) and narrowed

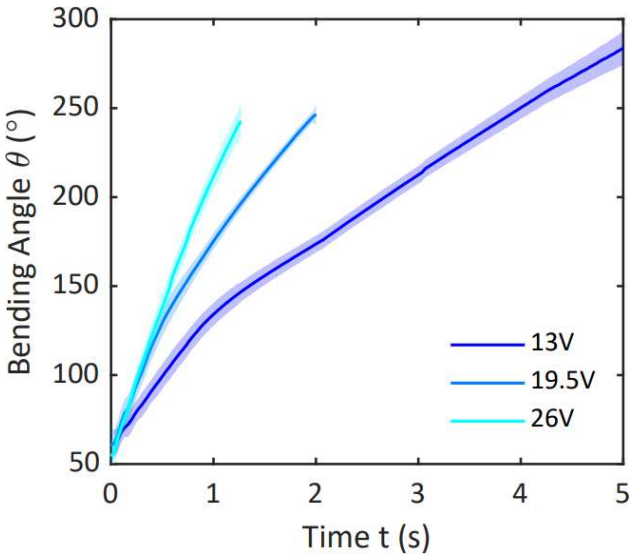

Figure 4.7: Bending angle vs time for a shape morphing module at various voltages. Note the nonlinearity is due to external forces present because this data was collected from the fully built robot standing up from a crawling configuration.

it down to three achievable modes: walking, crawling, and a shimmy type mode across a beam that we refer to as climbing. The robots walking mode of locomotion uses a dynamic trotting gait (Figure 4.8a), where the front-right and back-left legs step in unison and the front-left and back-right are in unison and start exactly one half of a step cycle after the preceding pair. Similarly, the climbing mode uses a bounding or inching type gait (Figure 4.8c) where both front legs are paired and both back legs are paired, each pair offset by one half-cycle later. The crawling mode employs a fully symmetric static gait where all four feet work in unison.

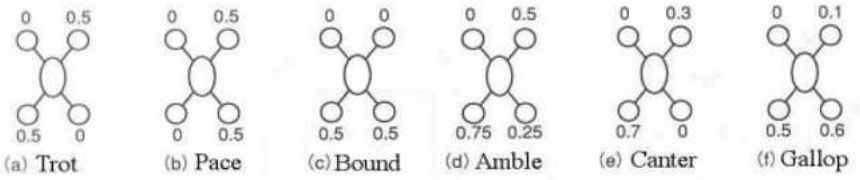

Figure 4.8: Various patterns of quadrupedal locomotion. The number by each foot corresponds to the proportion of time of one cycle that the foot begins its loop trajectory. Figure from reference [11].

4.4.2 Design and Fabrication

The last step in the project aimed to incorporate the 3D bending modules and the SMMs to make a four-legged robot. To keep the robot lightweight and simple, we decided to keep the controls and power off of the robot and use a tether to supply current to the TCAs and heating elements. We needed to ensure that there were enough SMMs connected in parallel to produce adequate force to overcome the friction from the ground and lift the robot into a standing position. We needed to be able to simultaneously supply two different voltages, one appropriate for the legs and one for the shape morphing body. Finally, we needed the open-loop control to be simple and easy to use, yet versatile enough that a user could call any of more than 20 routines on demand.

As with most of the prototype and light-duty end-use parts, we opted to use additive manufacturing to make the robot body clips as it is fast and affordable. For the robot body, which acts to hold the SMMs and 3D bending modules in place, we selected PLA as it is easy to print with and much more durable than SLA resin. All of the modules were designed to be press-fit together to avoid the weight and complexity that comes with using hardware.

Mechanical Components

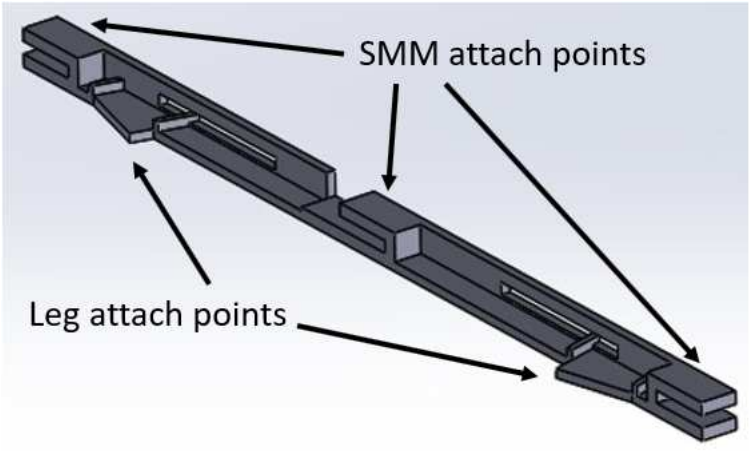

Figure 4.9: CAD model of one of the symmetrical body clips that hold the SMM and legs into position.

The body pieces (Figure 4.9) were designed so that the robot would be symmetric about its sagittal and coronal planes. The two identical body pieces are 95 mm in length and work together to hold three SMMs in parallel. There are channels to connect the body mount clips aligned to hold the legs 15°from parallel with the coronal plane, which increases the size of the robot base and acts to stabilize it from tipping. The left and right body pieces each have a piece of 26 gauge copper wire attached along its length which function as the common negative and positive (respectively) voltage rails for the SMM heating elements.

Electrical System

The simple, open-loop control electrical system was designed to be used manually by an operator. An Arduino Micro microcontroller simultaneously controls a 12 V power supply for the SMMs and a 50 V power supply for the 3D bending legs. Six Pololu DRV8835 motor drivers are used to supply current directly to the 12 TCAs that make up the legs, and a 24 V Pololu Dual Channel motor driver supplies current to the heating elements and three TCAs that make up the SMMs. The tether is made of sixteen 1 m long strands of insulated 34 gauge magnet wire, and the common ground is made of a 1m length strand of 28 gauge copper wire. Each wire in the tether has a JST pin soldered to one side and a JST socket soldered to the other.

The Arduino program leverages Serial Monitor as an interactive controller by taking a keyboard input and outputting a corresponding sub-routine. For instance, keys 1,2,3,4,5,6 independently actuate Left TCAs 1,2,3 and Right TCAs 1,2,3, respectively. The operator can independently activate the heating elements for the SMMs and all 15 TCAs, which is useful for testing each actuator and measuring its resistance. We built sub-routines for standing the robot up, laying it down, mounting a beam, crawling, climbing, and walking using various gaits. Having each TCA on a pulse width modulation (PWM) pin enables us to tune the voltage it receives so that we can mitigate minor discrepancies in TCA resistance. Unfortunately, an Arduino Micro only has 7 PWM pins but as a workaround we used the "SoftPWM" library which allows a user to simulate pulse width modulation on any pin.

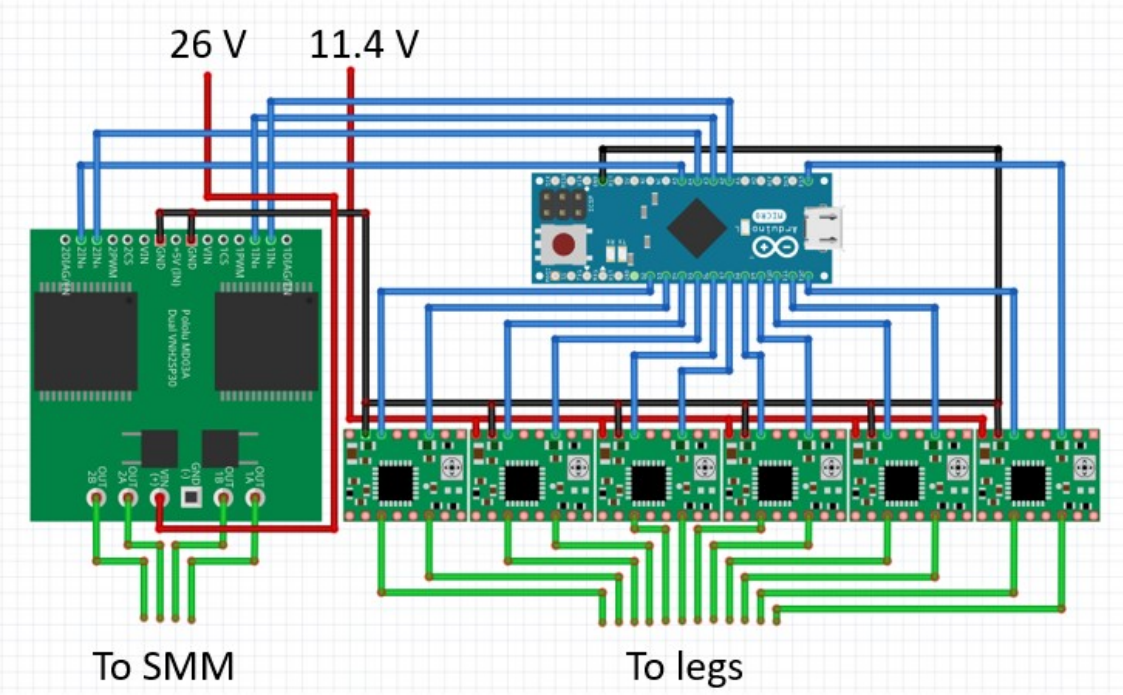

Figure 4.10: A schematic of the electrical components used to control the robot. The microcontroller is an Arduino micro and power is distributed using six Pololu DRV8835 motor drivers and a Pololu High Voltage motor driver.

4.4.3 Results

After building four 3D bending legs and three SMMs, the robot was assembled and all of the TCAs were trained. We began to realize morphing from one body type to another and executing various gaits and modes of locomotion, starting from the simplest function of crawling and moving on to progressively more difficult ones.

Crawling

The simplest of the three modes of locomotion that we could execute was crawling. We define crawling as a static gait because dynamic forces such as momentum and inertia do not affect the motion and because each step cycle can occur independently. To execute the crawling mode of locomotion, the robot must be in a lying down body configuration, with the SMMs minimally bent as seen in Figure 4.11. When heated, the shape memory polymers recovery force will morph the robot body into a lying down configuration from standing or gripping a beam. It is important that

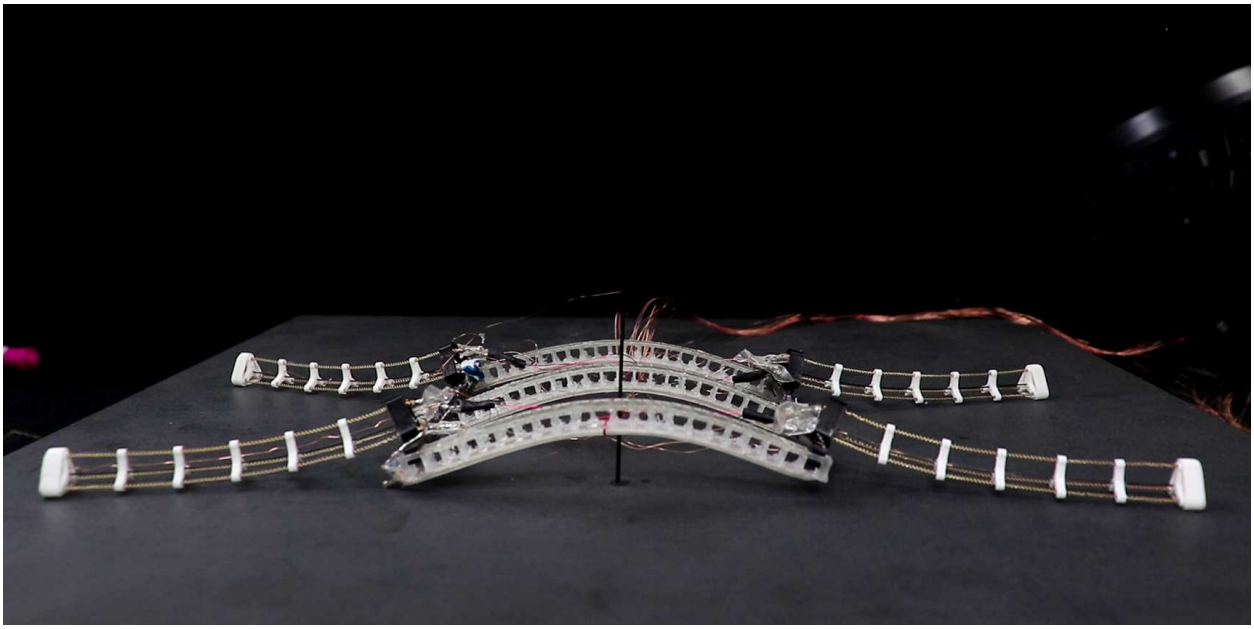

Figure 4.11: The robot in the lying down body configuration, in order to execute crawling locomotion.

the legs were not bent so far that the feet could not lift completely off the surface, as that would impede body movement. Also, note that the legs are stiff enough to be able to hold the exposed silicone surface of the robot's body off of the walking surface as it has a high friction coefficient and would not easily slide across a surface. In the lying down and crawling configuration the robot is 28 cm wide, 14 cm long and just 3.5 cm tall.

The crawling gait is the simplest of the three, with all four legs performing a step simultaneously. Figure 4.12 illustrates which TCAs are being actuated during each time step of a cycle. One cycle is split into six 600 ms time steps. For crawling, the first time step has TCA1 and TCA3 actuated which acts to push the feet down towards the crawling surface and lifts the robot body up. Next, only TCA3 is actuated for two time steps which pushes the foot down and back, propelling the robot forward. Next, only TCA2 is actuated which lifts the leg up and allows the robot body to rest back onto the crawling surface. During the following time step, TCA2 and TCA1 are actuated which lifts the robot's foot off the surface and steps forward. Finally, TCA1 alone is actuated bringing the foot to its furthest forward position, before the cycle starts over with a downward step. Crawling was the second slowest mode of locomotion as each step only moved the robot about 10% of its body length. A common measure of a robot's speed is how many body

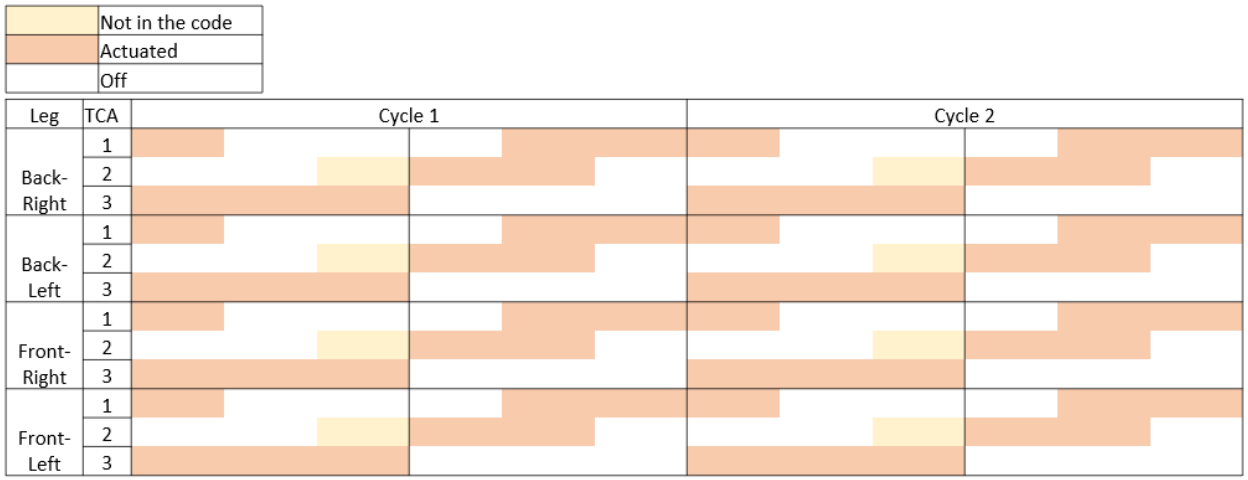

Figure 4.12: The TCA actuation pattern for two cycles of the crawling gait. All four legs are being actuated identically and in sync. Note the yellow portion is just to illustrate what a symmetrical foot trajectory loop would look like, we decided to make the actual foot trajectory asymmetrical so that it would be more efficient for locomotion.

lengths it can travel per minute and we determined the robot to be able to crawl approximately 2 body lengths per minute. The tether had very little effect on the crawling gait as long as it was able to move freely with the robot.

Walking

The walking mode of locomotion is more difficult to execute than crawling because it is a dynamic gait, where cycles have to be executed continuously and the robot has to maintain balance during the process. The robot must be in a standing configuration (as seen in Figure 4.13) to walk. The robot has to start in a lying down configuration before executing a stand-up maneuver(to go from the climbing grip to standing it must lie down first). The ideal SMM body angle for walking is between 110°and 150°. If the body bending angle is higher than 150°, the robot base is so small that the robot will lose balance and fall over during a step. If the body angle is lower than 110°, the legs are being loaded transversely with too much reaction force from the walking surface and are bent to the point where the TCAs cannot provide enough displacement to lift the feet off of the surface during steps. For our experiments, we used a body angle of 135°for walking. In a standing body configuration, the robot is 19 cm wide, 16 cm long, and stands 12 cm tall.

Figure 4.13: The multimodal shape morphing robot in a standing body configuration. The bending angle of the SMM body is approximately 145°, which provides an adequately large base that prevents the robot from toppling over while walking.

The walking gait was somewhat more complex than crawling because two pairs of feet have to work in sync, but with offset cycles. To maintain balance and symmetry throughout the dynamic movement, we broke each foot's step cycle into evenly spaced time steps and offset the two pairs' step initiation by a half cycle. Figure 4.14 illustrates this well. You can see the back-right and front-left legs are a synchronized pair, as are the back-left and front-right pair. Further, TCA actuation during the first half-cycle for one pair is identical to the second half-cycle of the other pair and vice-versa. This gait pattern is commonly known as a trot (Figure 4.8a). Fundamentally, the way this gait works is while one diagonal pair is lifting up and stepping forward, the other pair

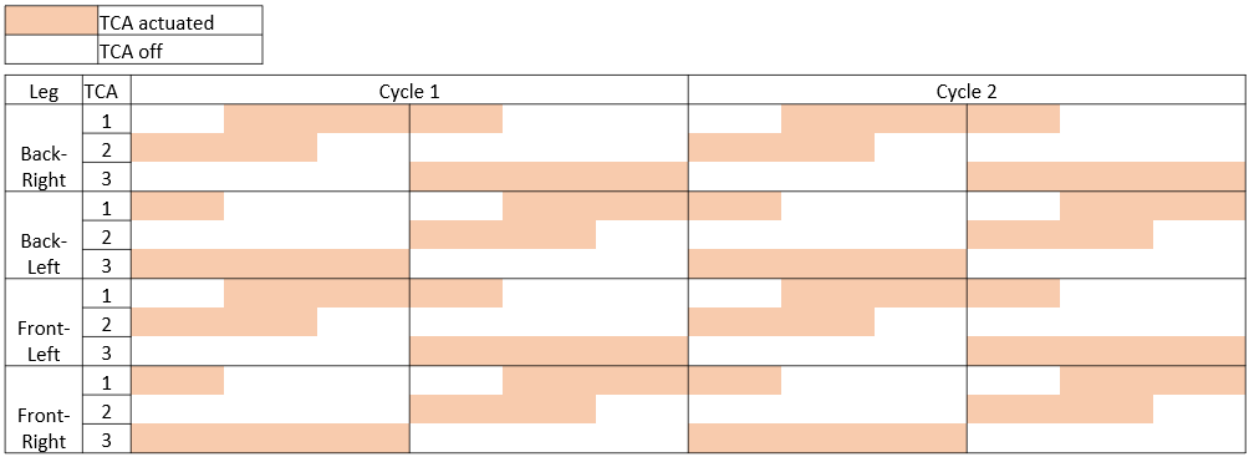

Figure 4.14: The TCA actuation pattern for two cycles of the walking gait. All four legs are being actuated identically and in sync. Note the yellow portion is just to illustrate what a symmetrical foot trajectory loop would look like, we decided to make the actual foot trajectory asymmetrical so that it would be more efficient for locomotion.

is pushing down to the walking surface to prevent the robot from sagging while the robot's entire weight is momentarily distributed across only two legs. Additionally, the cycle time has to be short enough that the robot does not tip while it is standing on two legs. Walking was the fastest mode of locomotion we were able to realize, at approximately 8 body lengths per minute.

Climbing

The climbing mode of locomotion was the most difficult to realize. It combines gripping a beam with a bound type inching gait. The working principle of the climbing mode is the robot body will bend to an angle of approximately 190°so that the legs effectively grip the beam (Figure 4.15). The feet must be supported vertically, but the ledge does not contribute to the movement. The forward motion is produced when the robot releases the grip of two legs, reaches forward, then grips again and pulls itself forward. Using the SMM to achieve a gripping force is difficult because the TCAs must be continuously actuated while the body cools, but if they are even 5°C too hot, the actuation force produced onto a rigid body will be high enough to catastrophically damage the TCA. The robot is approximately 7cm wide, 14cm long, and 15cm tall when gripping onto a beam.

The climbing gait was similar to the walking gait in that there are two pairs of synchronized legs operating a half-cycle out of sync with each other. The difference is that this gait uses the

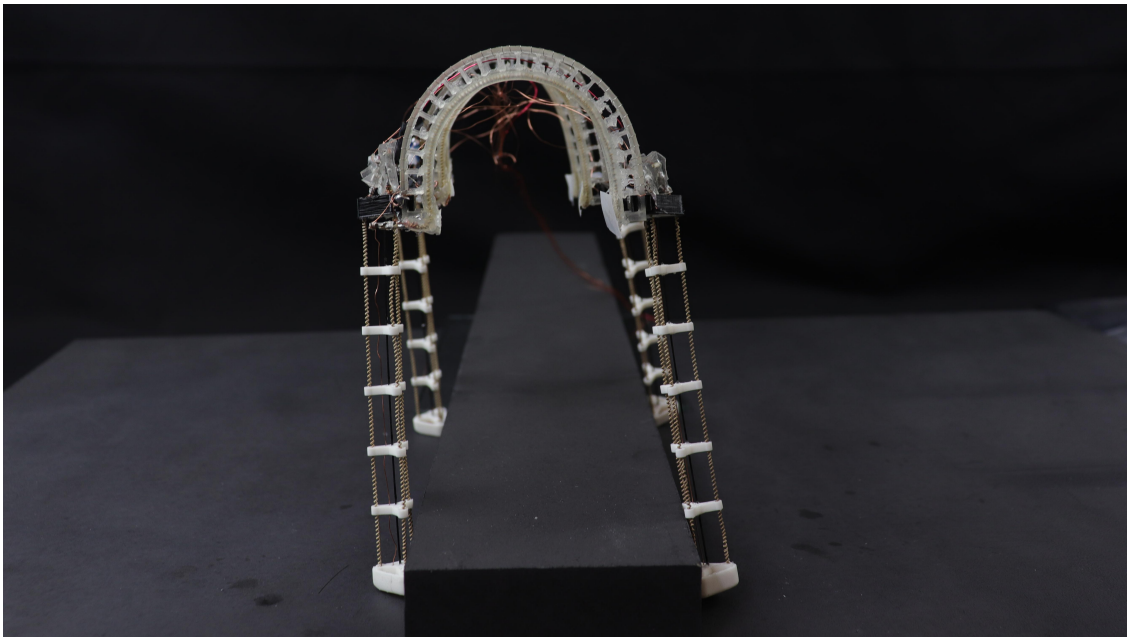

Figure 4.15: The robot gripping a beam in order to realize climbing. The bending angle shown here is approximately 190°so the the robots legs effectively grip the beam.

bound gait pattern (Figure 4.8c), where the front two legs are one pair and the back two legs are the other. Figure 4.16 is the actuation pattern for the climbing gait. You can see that, like walking, each cycle is symmetrical at the midpoint. This is crucial for movement because it means that when one pair of legs is gripping and pulling the robot forward, the other is releasing its grip allowing the robot to slide freely. Climbing proved to be the slowest gait we were able to realize at just 0.5 body lengths per minute.

Illustrative environment

After successfully realizing each mode of locomotion and morphing between the body configurations, we wanted to build an obstacle course to demonstrate our shape morphing, multimodal robots capabilities. Figure 4.17 was made from video snapshots of the robot traversing the environment. The robot started lying down on the left side of the obstacle course and proceeded to crawl under a pane of glass suspended 4cm above the platform. Once it cleared the window, the robot stood up, walked to the beam, and mounted it using the grip function. After mounting the

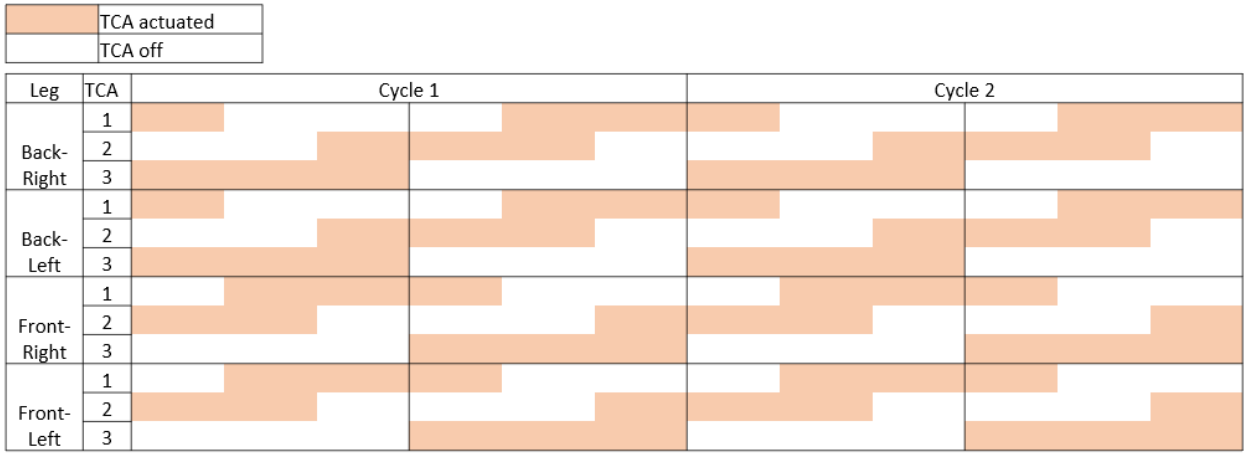

Figure 4.16: The TCA actuation pattern for two cycles of the climbing gait. All four legs are being actuated identically and in sync. Note the yellow portion is just to illustrate what a symmetrical foot trajectory loop would look like, we decided to make the actual foot trajectory asymmetrical so that it would be more efficient for locomotion.

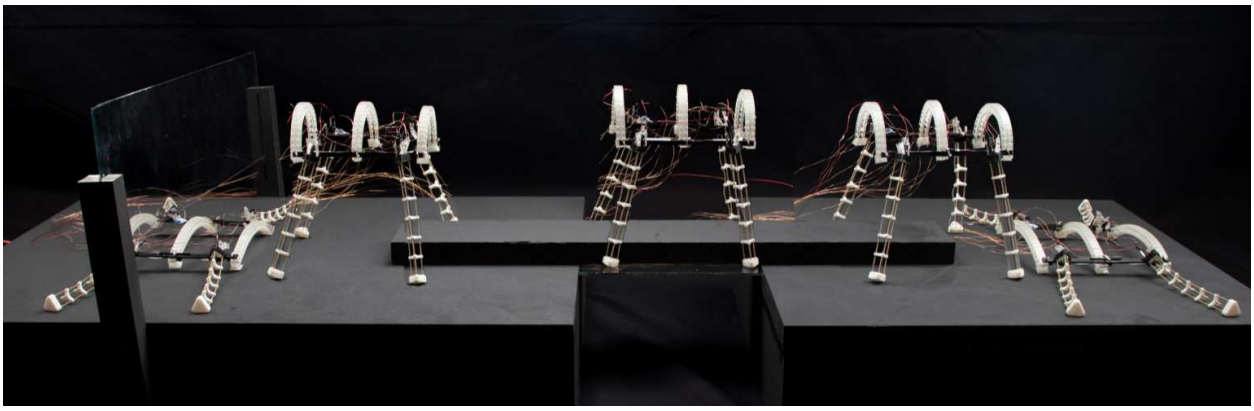

Figure 4.17: A diverse environment designed to demonstrate the capabilities of our multimodal robot.

beam the robot shimmied, or climbed, across the beam. Next, the robot dismounted the beam and walked to the rightmost platform where it returned to its original lying down body configuration.

4.4.4 Conclusion and future work

Each component was designed so that it could perform specific tasks, and after the robot was built, tested, refined, and rebuilt, we were able to accomplish the goal of making a robot that is one step closer to mimicking animalistic behavior. By altering the mechanical structure of our robot and employing various gaits, we were able to execute multiple modes of locomotion and traverse a relatively complex, technical environment. This project was the perfect application for TCAs

as the artificial muscles illustrate biomimicry on a micro-scale, and the robot does so on a macro scale.

Future work on this project could involve taking advantage of the TCAs sensory function to implement closed-loop control. It may involve scaling up the hardware so that the controls and power can be brought on board. There is also room to further refine the components so they work more effectively and robustly by using no more than 80% of the actuator capabilities.

Chapter 5

Conclusions and Future Work

5.1 Conclusions

There are many open avenues of exploration and invention in the field of soft robotics. There are also many practical applications for soft robotic actuators and sensors, partially because they are lightweight, affordable, and generally safer for human-robot interaction because of their highly compliant nature. The advent of free stroke twisted and coiled actuators was crucial in our work as they allowed us to embed TCAs into soft bodies without deforming them. They also produce much more displacement from a non-preloaded condition, which was leveraged in our 3D bending and shape morphing modules. Further, free stroke TCAs have a high lifespan (> 100,000 cycles) and have a much faster cyclic rate than other artificial muscles, especially when active cooling is implemented.

Our TCA manufacturing machine was instrumental not only in the fabrication and characterization of various TCAs but also in producing enough high-quality TCAs to use in various robots and robotic components. The redesigned machine can make TCAs 300% longer than the previous design, with fewer defects, which is essential for components that need longer sections of TCA such as our shape morphing modules. The machine operator can easily change parameters such as the helical coiling angle by porting into the microcontroller and altering the Arduino code. Other parameters, such as the spring index can be changed by simply changing the diameter of the coiling mandrel. The machine was designed in such a way that it is easy and safe to operate. We also made a training video and detailed TCA fabrication instructions so that anybody could learn to make TCAs in a matter of minutes.

The TCA-driven tensegrity robot was a largely successful project. A previous research group attempted to make a six-link, spherical tensegrity robot but was unsuccessful because they were trying to use conventional TCAs, which could not produce enough force and displacement to

overcome the reaction force of antagonistically oriented TCAs that were installed under preloaded conditions. We were able to successfully realize steps from each of three possible unique starting and ending conditions: closed-to-open base triangle, closed-to-closed base triangle, and open-to-closed base triangle configurations.

The multimodal shape morphing robot project was also a success. After developing efficient and effective 3D bending modules to use as legs, the shape morphing modules, and body components, we assembled the robot and began to investigate various gaits and body configurations. We successfully realized three unique modes of locomotion (crawling, walking, climbing). We experimentally determined that walking is the fastest gait we could realize, but crawling and climbing are advantageous for traversing around obstacles and through various types of terrain. Finally, we designed and built an obstacle course to demonstrate the capabilities of the robot.

5.2 Future work

Although the TCA manufacturing machine project was largely successful, there is still room to make improvements. For instance, the lower pulley that holds the twisted thread would experience friction and occasionally result in a failure of the fabrication process. This could be remedied by implementing a free-floating weighted pulley. Additionally, increasing the diameter of the pulley from 0.75" to 1.5" would help to more evenly distribute the twist in the thread, resulting in more consistent performance across the length of a TCA. Future work for the TCA manufacturing machine could involve redesigning it so that it can make a continuous length of TCA. This could be done by simultaneously twisting the thread, wrapping the guide wire around the core, and coiling the twisted thread onto the mandrel. Although more complex, this technique would allow an operator to make TCAs longer than 1 m.

Future work for the tensegrity robot could include untethering it by bringing the power and controls on board. To address the issue of overcoming the tensile force of antagonistically oriented TCAs, we could design a different TCA with a larger spring index that would stretch more easily, or possibly use a different method of actuation. One proposed actuation method could utilize

servos to switch states of a bi-stable mechanism so that it quickly hits the ground and initiates a roll.

Some future work on the shape morphing robot may include replacing the 3D bending legs with a 3D shape morphing module so that we could put the robot in a fully rigid state and still realize the bending functionality when needed. We may utilize the TCAs displacement sensing capabilities so that we could implement closed-loop control of the bending modules. This would allow us to bend the module to a desired angle quickly without the potential of overheating and catastrophically damaging a TCA. Utilizing a more effective active cooling technique or a cold environment would allow us to increase the legs' cyclic rate and eventually aid in the realization of more dynamic gaits such as running or jumping.

Bibliography

[1] Sangbae Kim, Cecilia Laschi, and Barry Trimmer. Soft robotics: A bioinspired evolution in robotics. *Trends in biotechnology*, 31, 04 2013.

[2] Jonathan Rossiter and Helmut Hauser. Soft robotics - the next industrial revolution? [industrial activities]. *IEEE Robotics Automation Magazine*, 23(3):17–20, 2016.

[3] Panagiotis Polygerinos, Stacey Lyne, Zheng Wang, Luis Fernando Nicolini, Bobak Mosadegh, George M Whitesides, and Conor J Walsh. Towards a soft pneumatic glove for hand rehabilitation. In *2013 IEEE/RSJ International Conference on Intelligent Robots and Systems*, pages 1512–1517. IEEE, 2013.

[4] Pham Huy Nguyen, Saivimal Sridar, Wenlong Zhang, and Panagiotis Polygerinos. Design and control of a 3-chambered fiber reinforced soft actuator with off-the-shelf stretch sensors. *International Journal of Intelligent Robotics and Applications*, 1(3):342–351, 2017.

[5] Yong-Lae Park, Jobim Santos, Kevin G Galloway, Eugene C Goldfield, and Robert J Wood. A soft wearable robotic device for active knee motions using flat pneumatic artificial muscles. In *2014 IEEE International Conference on Robotics and Automation (ICRA)*, pages 4805–4810. IEEE, 2014.

[6] Filip Ilievski, Aaron D Mazzeo, Robert F Shepherd, Xin Chen, and George M Whitesides. Soft robotics for chemists. *Angewandte Chemie*, 123(8):1930–1935, 2011.

[7] F Javier Garcia Rubiales, Pablo Ramon Soria, Begoña C Arrue, and Anibal Ollero. Soft-tentacle gripper for pipe crawling to inspect industrial facilities using uavs. *Sensors*, 21(12):4142, 2021.

[8] Edward L White, Jennifer C Case, and Rebecca K Kramer. Multi-mode strain and curvature sensors for soft robotic applications. *Sensors and Actuators A: Physical*, 253:188–197, 2017.

[9] Michael Meller, Boris Kogan, Matthew Bryant, and Ephrahim Garcia. Model-based feedforward and cascade control of hydraulic mckibben muscles. *Sensors and Actuators A: Physical*, 275:88–98, 2018.

[10] Vanessa Sanchez, Conor J Walsh, and Robert J Wood. Textile technology for soft robotic and autonomous garments. *Advanced Functional Materials*, 31(6):2008278, 2021.

[11] Robert F Shepherd, Filip Ilievski, Wonjae Choi, Stephen A Morin, Adam A Stokes, Aaron D Mazzeo, Xin Chen, Michael Wang, and George M Whitesides. Multigait soft robot. *Proceedings of the national academy of sciences*, 108(51):20400–20403, 2011.

[12] Fionnuala Connolly, Panagiotis Polygerinos, Conor J Walsh, and Katia Bertoldi. Mechanical programming of soft actuators by varying fiber angle. *Soft Robotics*, 2(1):26–32, 2015.

[13] Eric Acome, Shane K Mitchell, TG Morrissey, MB Emmett, Claire Benjamin, Madeline King, Miles Radakovitz, and Christoph Keplinger. Hydraulically amplified self-healing electrostatic actuators with muscle-like performance. *Science*, 359(6371):61–65, 2018.

[14] Philipp Rothemund, Nicholas Kellaris, Shane K Mitchell, Eric Acome, and Christoph Keplinger. Hasel actuators: Hasel artificial muscles for a new generation of lifelike robots—recent progress and future opportunities (adv. mater. 19/2021). *Advanced Materials*, 33(19):2170149, 2021.

[15] Zhijian Wang, Kai Li, Qiguang He, and Shengqiang Cai. A light-powered ultralight tensegrity robot with high deformability and load capacity. *Advanced Materials*, 31(7):1806849, 2019.

[16] Timothy J White and Dirk J Broer. Programmable and adaptive mechanics with liquid crystal polymer networks and elastomers. *Nature materials*, 14(11):1087–1098, 2015.

[17] Kyeong Ho Cho, Min Geun Song, Hosang Jung, Jungwoo Park, Hyungpil Moon, Ja Choon Koo, Jae-Do Nam, and Hyouk Ryeol Choi. A robotic finger driven by twisted and coiled polymer actuator. In *Electroactive Polymer Actuators and Devices (EAPAD) 2016*, volume 9798, page 97981J. International Society for Optics and Photonics, 2016.

[18] Xintian Tang, Kai Li, Yingxiang Liu, Dong Zhou, and Jianguo Zhao. A soft crawling robot driven by single twisted and coiled actuator. *Sensors and Actuators A: Physical*, 291:80–86, 2019.

[19] Xintian Tang, Kai Li, Yingxiang Liu, Dong Zhou, and Jianguo Zhao. A general soft robot module driven by twisted and coiled actuators. *Smart Materials and Structures*, 28(3):035019, 2019.

[20] Jiefeng Sun, Brandon Tighe, Yingxiang Liu, and Jianguo Zhao. Twisted-and-coiled actuators with free strokes enable soft robots with programmable motions. *Soft robotics*, 8(2):213–225, 2021.

[21] YaKun ZHANG, Yu ZHANG, Bo LI, and GuiMin CHEN. Progress of twisted and coiled polymer fiber artificial muscles and its application in soft robots. *SCIENTIA SINICA Technologica*, 51(2):119–136, 2020.

[22] Jean-Baptiste Chossat, Daniel KY Chen, Yong-Lae Park, and Peter B Shull. Soft wearable skin-stretch device for haptic feedback using twisted and coiled polymer actuators. *IEEE transactions on haptics*, 12(4):521–532, 2019.

[23] Dong Zhou, Yingxiang Liu, Xintian Tang, Jin Sun, and Jie Deng. A lightweight and multi-motion crawling tensegrity robot driven by twisted artificial muscles. *IEEE Transactions on Industrial Electronics*, 2021.

[24] Lianjun Wu, Monica Jung de Andrade, Tarang Brahme, Yonas Tadesse, and Ray H Baughman. A reconfigurable robot with tensegrity structure using nylon artificial muscle. In *Active and Passive Smart Structures and Integrated Systems 2016*, volume 9799, page 97993K. International Society for Optics and Photonics, 2016.

[25] Kyeong Ho Cho, Youngeun Kim, Sang Yul Yang, Kihyeon Kim, Jae Hyeong Park, Hugo Rodrigue, Hyungpil Moon, Ja Choon Koo, Hyouk Ryeol Choi, et al. Artificial musculoskeletal

actuation module driven by twisted and coiled soft actuators. *Smart Materials and Structures*, 28(12):125010, 2019.

[26] Brandon PR Edmonds and Ana Luisa Trejos. Stiffness control of a nylon twisted coiled actuator for use in mechatronic rehabilitation devices. In *2017 International Conference on Rehabilitation Robotics (ICORR)*, pages 1419–1424. IEEE, 2017.

[27] Seyed M Mirvakili and Ian W Hunter. Artificial muscles: Mechanisms, applications, and challenges. *Advanced Materials*, 30(6):1704407, 2018.

[28] Carter S Haines, Márcio D Lima, Na Li, Geoffrey M Spinks, Javad Foroughi, John DW Madden, Shi Hyeong Kim, Shaoli Fang, Mônica Jung de Andrade, Fatma Göktepe, et al. Artificial muscles from fishing line and sewing thread. *science*, 343(6173):868–872, 2014.

[29] Dong Zhou, Yingxiang Liu, Xintian Tang, Jin Sun, and Jie Deng. A lightweight and multi-motion crawling tensegrity robot driven by twisted artificial muscles. *IEEE Transactions on Industrial Electronics*, pages 1–1, 2021.

[30] Farzad Karami and Yonas Tadesse. Modeling of twisted and coiled polymer (tcp) muscle based on phenomenological approach. *Smart Materials and Structures*, 26(12):125010, 2017.

[31] Yara Almubarak and Yonas Tadesse. Twisted and coiled polymer (tcp) muscles embedded in silicone elastomer for use in soft robot. *International Journal of Intelligent Robotics and Applications*, 1(3):352–368, 2017.

[32] Sang Yul Yang, Kyeong Ho Cho, Youngeun Kim, Min-Geun Song, Ho Sang Jung, Ji Wang Yoo, Hyungpil Moon, Ja Choon Koo, Hyouk Ryeol Choi, et al. High performance twisted and coiled soft actuator with spandex fiber for artificial muscles. *Smart Materials and Structures*, 26(10):105025, 2017.

[33] Kihyeon Kim, Kyeong Ho Cho, Ho Sang Jung, Sang Yul Yang, Youngeun Kim, Jae Hyeong Park, Hoyoung Jang, Jae-Do Nam, Ja Choon Koo, Hyungpil Moon, et al. Double helix

twisted and coiled soft actuator from spandex and nylon. *Advanced Engineering Materials*, 20(11):1800536, 2018.

[34] Sarah A Horton and Patrick Dumond. Consistent manufacturing device for coiled polymer actuators. *IEEE/ASME Transactions on Mechatronics*, 24(5):2130–2138, 2019.

[35] Carter S Haines, Na Li, Geoffrey M Spinks, Ali E Aliev, Jiangtao Di, and Ray H Baughman. New twist on artificial muscles. *Proceedings of the National Academy of Sciences*, 113(42):11709–11716, 2016.

[36] Huai-Ti Lin, Gary G Leisk, and Barry Trimmer. Goqbot: a caterpillar-inspired soft-bodied rolling robot. *Bioinspiration & biomimetics*, 6(2):026007, 2011.

[37] Ali Rafie Ravandi. *Characterizing the behavior of nylon actuators and exploring methods for manufacturing them to get the highest amount of output*. PhD thesis, University of British Columbia, 2018.

[38] Yi-Wei Huang, Wen-Shin Lee, Yu-Fan Chuang, Wenxin Cao, Fuqian Yang, and Sanboh Lee. Time-dependent deformation of artificial muscles based on nylon 6. *Materials Science and Engineering: C*, 98:445–451, 2019.

[39] Antonello Cherubini, Giacomo Moretti, Rocco Vertechy, and Marco Fontana. Experimental characterization of thermally-activated artificial muscles based on coiled nylon fishing lines. *Aip Advances*, 5(6):067158, 2015.

[40] Kyunam Kim. *On the locomotion of spherical tensegrity robots*. University of California, Berkeley, 2016.

[41] Michael Hutson and Adam Ward. *Oxford textbook of musculoskeletal medicine*. Oxford University Press, 2015.

[42] Donald E Ingber. Tensegrity i. cell structure and hierarchical systems biology. *Journal of cell science*, 116(7):1157–1173, 2003.

[43] John Rieffel and Jean-Baptiste Mouret. Adaptive and resilient soft tensegrity robots. *Soft robotics*, 5(3):318–329, 2018.

[44] Ali Abbas and Jianguo Zhao. Twisted and coiled sensor for shape estimation of soft robots. In *2017 IEEE/RSJ International Conference on Intelligent Robots and Systems (IROS)*, pages 482–487. IEEE, 2017.

[45] Yuusuke Koizumi, Mizuho Shibata, and Shinichi Hirai. Rolling tensegrity driven by pneumatic soft actuators. In *2012 IEEE International Conference on Robotics and Automation*, pages 1988–1993. IEEE, 2012.

[46] Shinichi Hirai, Yuusuke Koizumi, Mizuho Shibata, Minghui Wang, and Li Bin. Active shaping of a tensegrity robot via pre-pressure. In *2013 IEEE/ASME International Conference on Advanced Intelligent Mechatronics*, pages 19–25. IEEE, 2013.

[47] Morgan T Pope, Christopher W Kimes, Hao Jiang, Elliot W Hawkes, Matt A Estrada, Capella F Kerst, William RT Roderick, Amy K Han, David L Christensen, and Mark R Cutkosky. A multimodal robot for perching and climbing on vertical outdoor surfaces. *IEEE Transactions on Robotics*, 33(1):38–48, 2016.

[48] Wenqi Hu, Guo Zhan Lum, Massimo Mastrangeli, and Metin Sitti. Small-scale soft-bodied robot with multimodal locomotion. *Nature*, 554(7690):81–85, 2018.

[49] Ludovic Daler, Julien Lecoeur, Patrizia Bernadette Hählen, and Dario Floreano. A flying robot with adaptive morphology for multi-modal locomotion. In *2013 IEEE/RSJ International Conference on Intelligent Robots and Systems*, pages 1361–1366. IEEE, 2013.

[50] Yasuhiro Fukuoka, Yasushi Habu, and Takahiro Fukui. A simple rule for quadrupedal gait generation determined by leg loading feedback: a modeling study. *Scientific reports*, 5(1):1–11, 2015.

[51] Dai Owaki and Akio Ishiguro. A quadruped robot exhibiting spontaneous gait transitions from walking to trotting to galloping. *Scientific reports*, 7(1):1–10, 2017.